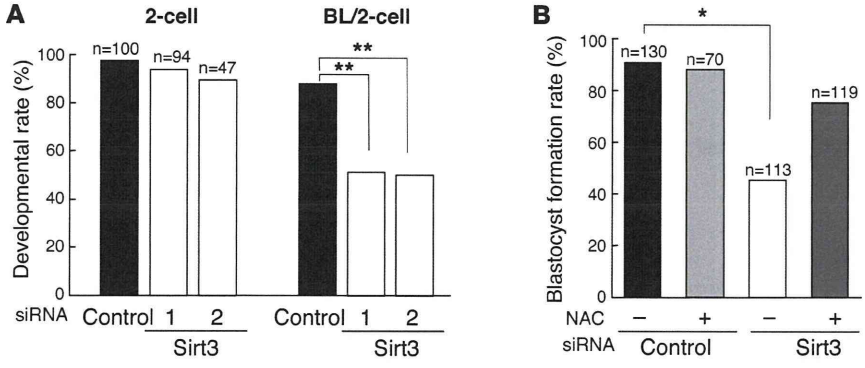

Figure 6
RNAi-mediated Sirt3 knockdown adversely affects preimplantation developmental outcomes. (**A**) Intracytoplasmic injection of both stealth Sirt3 siRNAs led to decreased blastocyst formation rate in preimplantation embryos. Data are derived from 4 independent experiments. (**B**) Sirt3 siRNA–induced decrease in blastocyst formation rate was suppressed by treatment with NAC. Data are derived from 6 independent experiments. Statistical assessments were performed by applying Ryan's multiple-comparison test. $*P < 0.05$; $**P < 0.001$.

conditions abolished Sirt3 knockdown–induced developmental defects. These findings suggest that Sirt3 plays a protective role against oxidative stress–induced developmental arrest in IVF and in vitro–cultured preimplantation embryos.

Within mitochondria, the primary sites of ROS generation are complexes I and III of the electron transport chain (12–14). Accumulation of electron donors as a result of reduced electron flow and increased oxygen concentration is supposed to cause excessive generation of superoxide as the primary product (44). Enhanced ROS production induced by Sirt3 inactivation was blocked by stigmatellin, which inhibits electron flux at complexes I and III (33). In this vein, it is noteworthy that Sirt3 deficiency led to inhibition of complex I activity, possibly through hyperacetylation of multiple components of complex I, such as NDUFA9 (30). Thus, alterations in electron transfer activity of complex I may be responsible for increased mitochondrial ROS generation in Sirt3-knockdown embryos. In addition, Sirt3 expression was upregulated by H_2O_2 in preimplantation embryos. This may serve as a feedback mechanism to regulate intracellular ROS levels.

Recent studies have shown that Sirt3 interacts with Foxo3a, a forkhead box–containing transcription factor, to upregulate the expression of manganese superoxide dismutase and catalase, thereby decreasing intracellular ROS levels in cardiomyocytes and suppressing cardiac hypertrophy (45). Upon deacetylation by Sirt3, Foxo3a translocates to the nucleus to transactivate the antioxidant genes (45). However, our preliminary experiments did not detect any differences in Foxo3a localization or the expression of catalase and Mn-superoxide dismutase genes, downstream targets of Foxo3a, between control and Sirt3-knock-

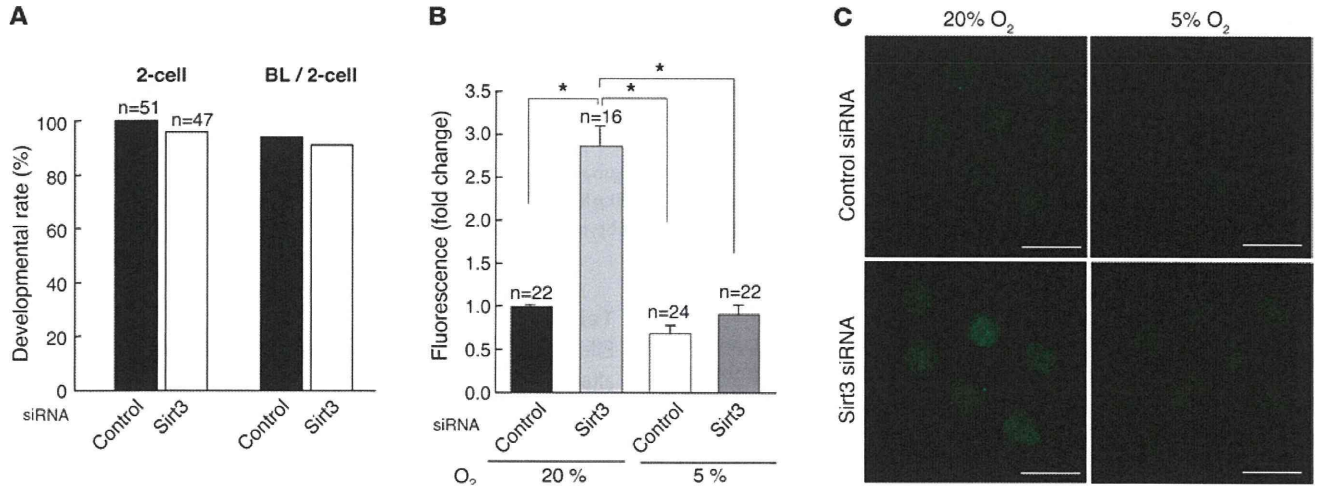

Figure 7
Low-oxygen conditions abolish developmental defects induced by Sirt3 knockdown. (**A**) Intracytoplasmic injection of Sirt3 siRNA did not affect 2-cell and blastocyst formation rates in low-oxygen (5% O_2) conditions. Data are derived from 4 independent experiments. (**B**) Effects of siRNA-mediated Sirt3 knockdown on intracellular ROS levels, as estimated by CM-H_2DCFDA fluorescence intensity, in 20% and 5% O_2 conditions. Sirt3 knockdown–induced ROS increases were canceled in 5% O_2 conditions. Data are derived from 3 independent experiments. Statistical assessments were performed by applying Games-Howell test. $*P < 0.05$. (**C**) Representative images of CM-H_2DCFDA fluorescence in embryos analyzed in **B**. Scale bar: 100 μm.

Table 1
Effect of maternal *Sirt3* genotype on IVF rate

Genotype		IVF (*n*)		Fertilization rate
Sperm	Egg	Fertilized	Unfertilized	
Sirt3$^+$	*Sirt3*$^+$	51	19	73%
Sirt3$^+$	*Sirt3*$^-$	62	28	69%
Sirt3$^-$	*Sirt3*$^+$	62	10	86%
Sirt3$^-$	*Sirt3*$^-$	65	31	68%

Cochran-Mantel-Haenszel χ^2 test stratified on sperm genotype.
$\chi^2 = 4.701$; $P = 0.030$; odds ratio 1.813.

down embryos (our unpublished observations), which indicates that Foxo3a might not be contributing to the protective role of Sirt3 against oxidative stress in preimplantation embryos.

Involvement of p53 in ROS-induced preimplantation developmental arrest in Sirt3-deficient embryos. Mitochondrial ROS increase in Sirt3-knockdown embryos is accompanied by upregulation of p53 expression. Furthermore, siRNA-induced p53 knockdown improved developmental outcome in Sirt3-knockdown embryos.

Under normal conditions, levels of p53 protein are kept low because of its short half-life through the ubiquitin-proteasome degradation pathway, mediated by E3 ubiquitin ligase Mdm2, in preimplantation embryos as well as in various somatic cells (35, 46). Upon stress conditions, modification (e.g., phosphorylation) of p53 and/or Mdm2 causes p53 stabilization and activation by inhibiting the p53-Mdm2 interaction (35). In in vitro–cultured preimplantation embryos, the latency of p53 is maintained by the phosphatidylinositol-3′-kinase/Akt–mediated activation of Mdm2 (46). Perturbation of this pathway, as well as Mdm2 inactivation, results in the accumulation of p53 and developmental arrest (46–48), which indicates that the latency of p53 is important for normal preimplantation development. Although mitochondrial ROS has proved to contribute to stress-induced p53 activation in some somatic cells (49), the involvement of p53 in the stress response of preimplantation embryos has been controversial (50, 51). The present study indicated that p53 is involved in developmental arrest induced by mitochondrial ROS in Sirt3-knockdown embryos.

Sirt3-related mechanisms independent of ROS may be involved in p53 activation in cooperation with mitochondrial ROS. AMPK, which responds to an increase in AMP/ATP ratio during calorie restriction, can activate p53 by increasing transcription of *p53* and through direct phosphorylation of p53 (52, 53). This pathway might be activated in Sirt3-deficient embryos, in which mitochondrial ATP synthesis is possibly decreased (30). Another possibility is that Sirt3 may deacetylate p53 as well as Sirt1 (54, 55), and, in the absence of Sirt3, acetylated p53 may accumulate in embryos. p53 acetylation is induced in response to stress and causes its activation and stabilization (54–56). Furthermore, p53 has recently been reported to localize to mitochondria (57). Thus, it would be interesting to test whether acetylated p53 could serve as a substrate for Sirt3 deacetylase activity.

The present study showed that expression of *Nanog* was downregulated in Sirt3-knockdown or -knockout embryos, and expression of *p21* was upregulated. Although it may simply reflect developmental delay, this finding is compatible with previous reports that p53 suppresses *Nanog* expression in ES cells after DNA damage, which may serve as a mechanism to maintain genomic stability in ES cells (39, 40). We speculate that, in the absence of Sirt3, p53 is activated by excessive mitochondrial ROS to prevent the generation of embryos carrying serious mutations partly through changes in p21 and Nanog activity.

Conclusion. We have identified Sirt3 as a protective factor against stress in preimplantation development under IVF and in vitro culture conditions. Sirt3 deficiency caused increased mitochondrial ROS production and subsequent developmental arrest attributed to p53 activation in preimplantation embryos. The present findings may contribute to the understanding of preimplantation biology and give a clue to the better outcome of assisted reproductive technologies.

Methods

Mice. ICR mice from Charles River Laboratories Japan Inc. were used in all experiments, except for those using C57BL6-background Sirt3-knockout mice with the *Sirt3*$^{Gt(neo)218Lex}$ allele (here referred to as *Sirt3*$^-$), which were generated by Lexicon Genetics and obtained from Mutant Mouse Regional Resource Centers. Mice were housed in an environmentally controlled room at 23°C ± 2°C, with 50%–60% relative humidity, under a 12-hour light/12-hour dark cycle. All animal experiments were approved by the Animal Care and Use Committee of the University of Tokyo and were performed in accordance with institutional guidelines.

Collection of eggs, IVF, and assessment of in vitro development. Female mice (8–10 weeks old) were superovulated with intraperitoneal injections of 7.5 IU pregnant mare serum gonadotropin (PMSG; Teikoku Hormone Mfg.) and, 48 hours later, 7.5 IU human chorionic gonadotropin (hCG; Teikoku Hormone Mfg.). Eggs were recovered from the oviducts 20 hours after hCG injection, and cumulus cells were extensively dispersed with 1 mg/ml hyaluronidase (Sigma-Aldrich). Sperm were expelled from the cauda epididymis of male mice into 200 μl human tubal fluid (HTF) medium and incubated under mineral oil for 1–2 hours at 37°C to capacitate. A sperm suspension at a concentration of 6–7 × 10^5 sperm/ml was used to inseminate eggs in a 200-μl drop of HTF medium under mineral oil. After coincubation with sperm for 6 hours, the inseminated eggs were washed and cultured in 50-μl droplets of potassium simplex optimized medium (KSOM; Specialty Media) under mineral oil at 37°C in humidified air containing 5% CO_2. Experiments at low oxygen concentration were performed in a humidified airtight chamber maintained at 37°C and flushed with a mixture of 5% O_2 and 5% CO_2 balanced with N_2. In experiments with inhibitors, each medium was supplemented with 5 mM nicotinamide (Sigma-Aldrich), 200 μM sirtinol (Calbiochem), 2 μM BML-210 (Biomol), 500 μM NAC (Wako), or DMSO (Sigma-Aldrich) alone. Cleavage and embryo development were examined every 24 hours.

Table 2
Effect of maternal *Sirt3* genotype on blastocyst formation rate after IVF

Genotype		Blastocysts (*n*)		Formation rate
Sperm	Egg	Formed	Unformed	
Sirt3$^+$	*Sirt3*$^+$	30	1	97%
Sirt3$^+$	*Sirt3*$^-$	19	13	59%
Sirt3$^-$	*Sirt3*$^+$	39	3	93%
Sirt3$^-$	*Sirt3*$^-$	30	15	67%

Cochran-Mantel-Haenszel χ^2 test stratified on sperm genotype.
$\chi^2 = 19.263$; $P < 0.001$; odds ratio 9.666.

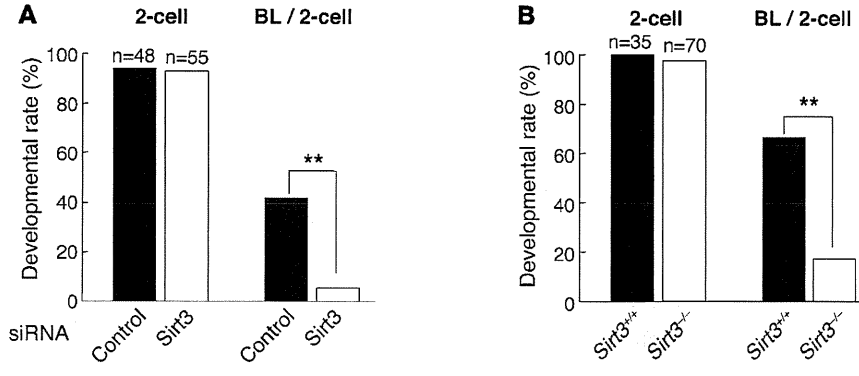

Figure 8
Parthenogenetic development is blocked by Sirt3 deficiency. (**A**) After Sr^{2+} activation for 4.5 hours, eggs that formed 2 pronuclei were injected with control or Sirt3 siRNA, and the rates of 2-cell and blastocyst formation were evaluated. (**B**) Eggs collected from wild-type and *Sirt3*$^{-/-}$ female mice underwent parthenogenetic activation. Data are derived from 4 (**A**) or 2 (**B**) independent experiments. Statistical assessments were performed by applying Fisher's exact test. $^{**}P < 0.001$.

Assessment of in utero development. Female ICR mice (8–10 weeks old) were bred with vasectomized ICR males to stimulate pseudopregnancy. Vaginal plug–positive females were used as recipients. Cultured embryos were transferred to recipients on day 0.5 of pseudopregnancy according to standard procedures. 7–10 embryos were transferred into each fallopian tube. Recipients were subjected to cesarean section on day 18.5 to determine the developmental competence of transferred embryos.

Parthenogenetic activation of eggs. ICR mouse eggs were activated by a 3- to 4-hour treatment with 10 mM Sr^{2+} prepared in Ca^{2+}-free M16 medium. Cytochalasin B (Sigma-Aldrich), an inhibitor of actin filament polymerization, was used to suppress the second polar body extrusion to generate diploid parthenotes. Activated eggs with 2 pronuclei, visualized under a differential interference contrast microscope, were defined as diploid parthenotes. Activated eggs were washed extensively and cultured in vitro under the same conditions as were IVF zygotes.

Plasmids. Mouse *Sirt1*, *Sirt2*, and *Sirt3* cDNAs were cloned by RT-PCR on total RNA from NIH 3T3 cells. For EGFP fusion constructs, cDNA fragments encompassing the open reading frame of *Sirt1*, *Sirt2*, and *Sirt3* were subcloned in frame into the pEGFP-N3 expression vector (Clontech). The fragments encoding the fusion constructs were then subcloned into pCRII-TOPO (Invitrogen) for in vitro transcription. The constructs were verified by sequencing.

Cell culture and transfection. NIH 3T3 cells were cultured in Dulbecco modified Eagle medium containing 10% fetal calf serum and antibiotics at 37°C in 5% CO_2. For siRNA transfection, cells were grown to 30%–50% confluence and treated with a mixture of siRNA and oligofectamine reagents (Invitrogen) according to the manufacturer's protocol.

Conventional RT-PCR. Female ICR mice (8–10 weeks old) were superovulated as above and used for collection of eggs or mated with ICR male mice to obtain early embryos at different stages. In some experiments, in vitro–cultured embryos and NIH 3T3 cells were collected at the indicated times. Samples were lysed in lysing buffer (Isogen; Nippon Gene), with volumes adjusted according to the number of eggs or embryos, and subjected to RNA extraction according to standard procedures. After reverse transcription with Quantiscript Reverse Transcriptase and RT Primer Mix (QuantiTect Reverse Transcription; Qiagen), PCR amplification was performed using specific primers listed in Supplemental Table 1. Thermal cycling was performed for 30–35 cycles

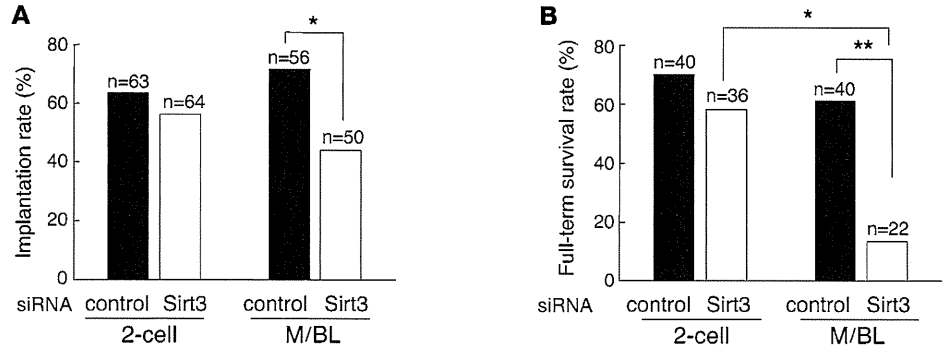

Figure 9
Long-term in vitro culture leads to decreased implantation and full-term survival rates in Sirt3-knockdown embryos. (**A** and **B**) Implantation rates (**A**) and full-term survival rates (**B**) of embryos injected with Sirt3 or control siRNA and transferred into pseudopregnant mice at the 2-cell or morula/blastocyst stage. Implantation sites and viability of fetuses were inspected by cesarean section 18 days after transfer. Implantation rate was estimated by the number of implantation sites; full-term survival rate was assessed by dividing the number of live pups by the number of implantation sites. Data are derived from 5 (2-cell embryo transfer) or 4 (morula/blastocyst transfer) independent experiments. Statistical assessments were performed by applying Ryan's multiple-comparison test. $^{*}P < 0.005$; $^{**}P < 0.001$.

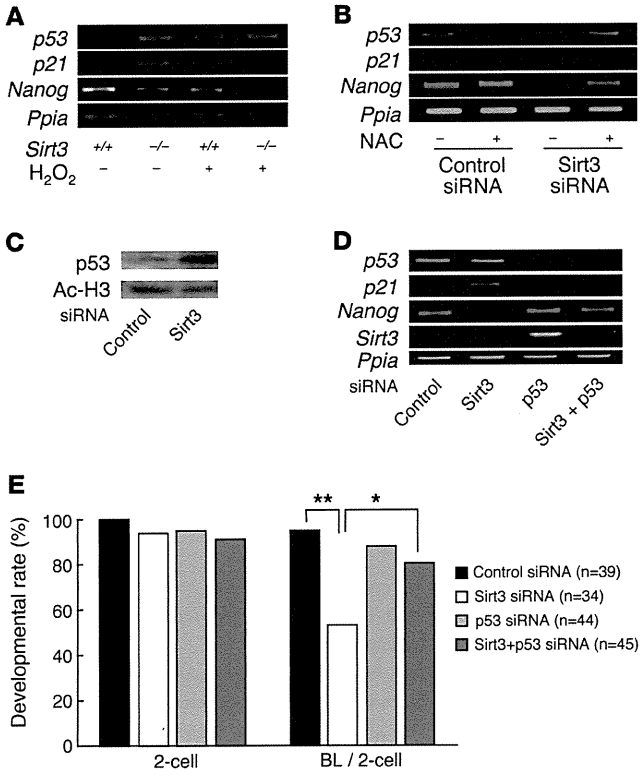

Figure 10

Involvement of p53 in developmental arrest of Sirt3-deficient preimplantation embryos. (**A**) *p53* and *p21* were upregulated in *Sirt3*$^{-/-}$ embryos as in H_2O_2-treated wild-type embryos. *Nanog* expression was decreased in *Sirt3*$^{-/-}$ embryos, and the decrease was enhanced by H_2O_2 stimulus. (**B**) Effects of Sirt3 knockdown and treatment with NAC on the expression of *p53* and its downstream genes. In Sirt3 siRNA–injected embryos, *p21* expression was upregulated, whereas *Nanog* expression was downregulated. These effects were blocked by NAC. (**C**) Western blotting analysis showing increased p53 protein levels in Sirt3-knockdown embryos at the morula stage. Signals for acetylated histone H3 (Ac-H3) served as an internal control. (**D**) Effects of p53 knockdown on Sirt3 siRNA–induced changes in the expression of genes downstream of p53. Sirt3 siRNA–induced *p21* upregulation and *Nanog* downregulation were blocked by siRNA-mediated p53 knockdown. *Ppia* expression served as an internal control in **A**, **B**, and **D**. (**E**) Effects of p53 knockdown on preimplantation developmental arrest in Sirt3-knockdown embryos. The rate of blastocyst formation was significantly improved by coinjection with p53 siRNA. Data are derived from 4 independent experiments. Statistical assessments were performed by applying Ryan's multiple-comparison test. $^{*}P < 0.05$; $^{**}P < 0.001$.

to maintain PCR conditions within the linear range of amplification before saturation was reached. Each cycle consisted of 30 seconds of denaturation at 94°C, 30 seconds of annealing at each annealing temperature (Supplemental Table 1), and 30 seconds of extension at 72°C. Signals for *Gapdh* and peptidylprolyl isomerase A (*Ppia*) expression served as internal controls.

Quantitative real-time PCR. Quantification of each mRNA level was performed by real-time RT-PCR analyses using a LightCycler (Roche) and Real-Time PCR Premix with SYBR Green (RBC Bioscience) following the manufacturers' protocols. Each cycle consisted of 10 seconds of denaturation at 94°C, 13–15 seconds of annealing at each annealing temperature (Supplemental Table 2), and 12–13 seconds of extension at 72°C. Thermal cycling was performed for 45–50 cycles. The second-derivative maximum method was adopted to determine the crossing points automatically for individual samples, and relative amounts of mRNA were calculated based on the crossing-point analysis. *Ppia* was used as an internal control. The result was expressed as fold change relative to control.

Western blotting. A pool of approximately 50 early embryos or NIH 3T3 cells was lysed in Laemmli buffer containing protease inhibitors, and then subjected to 12% SDS-PAGE. The separated proteins were transferred to a nylon membrane, which was then pretreated with 3% bovine serum albumin for blocking and incubated with primary antibodies as follows: rabbit anti-Sirt3 antibody (Abgent) for NIH 3T3 cell samples, rabbit anti-Sirt3 antibody from E. Verdin (UCSF, San Francisco, California, USA; ref. 26) for early embryo samples, and mouse anti-p53 antibody (BD Biosciences — Pharmingen). Blots were then incubated with anti-rabbit or anti-mouse IgG antibody conjugated to horseradish peroxidase (ICN). The protein bands were visualized using an ECL Plus Western Blotting Detection System (Amersham Pharmacia Biotech). The membrane was then washed and reblotted with anti-α-tubulin antibody (Sigma-Aldrich) or anti–acetylated histone H3 antibody (Cell Signaling Technology) for an internal control. Densitometric quantification was performed with ImageJ software (NIH).

RNAi. Chemically synthesized 25-nucleotide stealth RNAi duplex oligonucleotides were commercially obtained (Invitrogen). We selected 2 different sequences for each of the genes, *Sirt3* and *p53*, selected for the generation of siRNA: the sequences for siRNAs 1 and 2 corresponded, respectively, to nucleotides 355–379 and 386–410 of mouse *Sirt3* (GenBank accession no. NM_022433) and to nucleotides 985–1,009 and 165–189 of mouse *p53* (GenBank accession no. NM_011640; Supplemental Table 2). Stealth RNAi negative control HiGC (Invitrogen) was used as control siRNA. Approximately 10 pl of 20 μM siRNA was injected into the cytoplasm of fertilized eggs. The efficiency of gene knockdown was evaluated by RT-PCR with primers specific for mouse *Sirt3* and *p53* mRNA (Supplemental Table 1).

In vitro transcription and RNA microinjection. Preparation and injection of in vitro–transcribed mRNA were performed as previously described (58). Briefly, plasmids containing Sirt1-EGFP, Sirt2-EGFP, and Sirt3-EGFP fusion constructs and EGFP alone were linearized and used as templates for in vitro transcription using the T7 MessageMachine kit (Ambion). Synthesized RNA was further polyadenylated by yeast poly(A) polymerase (Amersham Biosciences) and resolved in 150 mM KCl with a final concentration of approximately 100 ng/μl. The diluted RNA was filtered, heated at 90°C for 1 minute, and cooled on ice. Then, approximately 10 pl RNA solution was injected into fertilized eggs through a glass micropipette. Embryos were grown to the 2-cell stage, at which time confocal images were obtained using a Nikon D-ECLIPSE C1 system.

Detection of intracellular ROS. To detect intercellular ROS in living embryos, we used CM-H_2DCFDA from Invitrogen. CM-H_2DCFDA was prepared in DMSO immediately prior to loading. Embryos were incubated with 10 μM CM-H_2DCFDA for 30 minutes and observed under a laser scanning confocal microscope (Nikon D-ECLIPSE C1), with an excitation wavelength of

480 nm and an emission wavelength of 505–530 nm. In some experiments, embryos were pretreated with the NAD(P)H oxidase inhibitor apocynin (100 μM) or the ubiquinol/cytochrome *c* oxidoreductase inhibitor stigmatellin (10 μM) for 30 minutes.

Statistics. Differences between 2 groups were analyzed by Mann-Whitney *U* test. Multiple comparisons between more than 2 groups were analyzed by 1-way ANOVA and post-hoc tests as indicated in the figure legends. Continuous data are presented as mean ± SEM. *P* values less than 0.05 were considered significant.

Acknowledgments

We thank Eric Verdin for Sirt3 antibody; Atsuo Ogura, Hiroshi Suzuki, and Kiyoshi Kita for helpful discussions and comments; Yuko Fujisawa for technical assistance; and Chisato Fujimoto for statistical analysis. This work was supported in part by Global COE Program (Integrative Life Science Based on the Study of Biosignaling Mechanisms); MEXT, Japan; grants-in-aid for scientific research from the Ministry of Education, Culture, Sports, Science and Technology of Japan; and grants-in-aid for scientific research from the Ministry of Health, Labor, and Welfare of Japan.

Received for publication December 14, 2009, and accepted in revised form June 9, 2010.

Address correspondence to: Hiroki Kurihara, Department of Physiological Chemistry and Metabolism, Graduate School of Medicine, University of Tokyo, 7-3-1 Hongo, Bunkyo-ku, Tokyo 113-0033, Japan. Phone: 81.3.5841.3498; Fax: 81.3.5684.4958; E-mail: kuri-tky@umin.ac.jp.

Nanao Horike's present address is: Animal Models of Human Diseases, National Institute of Biomedical Innovation, Osaka, Japan.

Tomokazu Amano's present address is: Developmental Genomics and Aging Section, Laboratory of Genetics, National Institute on Aging, NIH, Baltimore, Maryland, USA.

1. Matzuk MM, Lamb DJ. The biology of infertility: research advances and clinical challenges. *Nat Med.* 2008;14(11):1197–1213.
2. Smith S, Pfeifer SM, Collins JA. Diagnosis and management of female infertility. *JAMA.* 2003; 290(13):1767–1770.
3. Van Voorhis BJ. Clinical practice. In vitro fertilization. *N Engl J Med.* 2007;356(4):379–386.
4. Baird DD, Wilcox AJ, Weinberg CR. Use of time to pregnancy to study environmental exposures. *Am J Epidemiol.* 1986;124(3):470–480.
5. Witschi E. Natural control of fertility. *Fertil Steril.* 1968;19(1):1–14.
6. Van Blerkom J. Mitochondria in early mammalian development. *Semin Cell Dev Biol.* 2009; 20(3):354–364.
7. Wilding M, Coppola G, Dale B, Di Matteo L. Mitochondria and human preimplantation embryo development. *Reproduction.* 2009;137(4):619–624.
8. Thompson JG, McNaughton C, Gasparrini B, McGowan LT, Tervit HR. Effect of inhibitors and uncouplers of oxidative phosphorylation during compaction and blastulation of bovine embryos cultured in vitro. *J Reprod Fertil.* 2000;118(1):47–55.
9. Thouas GA, Trounson AO, Wolvetang EJ, Jones GM. Mitochondrial dysfunction in mouse oocytes results in preimplantation embryo arrest in vitro. *Biol Reprod.* 2004;71(6):1936–1942.
10. Trimarchi JR, Liu L, Porterfield DM, Smith PJ, Keefe DL. Oxidative phosphorylation-dependent and -independent oxygen consumption by individual preimplantation mouse embryos. *Biol Reprod.* 2000;62(6):1866–1874.
11. Van Blerkom J, Davis PW, Lee J. ATP content of human oocytes and developmental potential and outcome after in-vitro fertilization and embryo transfer. *Hum Reprod.* 1995;10(2):415–424.
12. Raha S, Robinson BH. Mitochondria, oxygen free radicals, disease and ageing. *Trends Biochem Sci.* 2000;25(10):502–508.
13. Zhang DX, Gutterman DD. Mitochondrial reactive oxygen species-mediated signaling in endothelial cells. *Am J Physiol Heart Circ Physiol.* 2007; 292(5):H2023–H2031.
14. Brookes PS, Yoon Y, Robotham JL, Anders MW, Sheu SS. Calcium, ATP, and ROS: a mitochondrial love-hate triangle. *Am J Physiol Cell Physiol.* 2004;287(4):C817–C833.
15. Covarrubias L, Hernandez-Garcia D, Schnabel D, Salas-Vidal E, Castro-Obregon S. Function of reactive oxygen species during animal development: passive or active? *Dev Biol.* 2008;320(1):1–11.
16. Ruder EH, Hartman TJ, Blumberg J, Goldman MB. Oxidative stress and antioxidants: exposure and impact on female fertility. *Hum Reprod Update.* 2008;14(4):345–357.
17. Agarwal A, Gupta S, Sekhon L, Shah R. Redox considerations in female reproductive function and assisted reproduction: from molecular mechanisms to health implications. *Antioxid Redox Signal.* 2008;10(8):1375–1403.
18. Liu L, Trimarchi JR, Keefe DL. Involvement of mitochondria in oxidative stress-induced cell death in mouse zygotes. *Biol Reprod.* 2000;62(6):1745–1753.
19. Finkel T, Deng CX, Mostoslavsky R. Recent progress in the biology and physiology of sirtuins. *Nature.* 2009;460(7255):587–591.
20. Schwer B, Verdin E. Conserved metabolic regulatory functions of sirtuins. *Cell Metab.* 2008;7(2):104–112.
21. Longo VD, Kennedy BK. Sirtuins in aging and age-related disease. *Cell.* 2006;126(2):257–268.
22. Imai S, Armstrong CM, Kaeberlein M, Guarente L. Transcriptional silencing and longevity protein Sir2 is an NAD-dependent histone deacetylase. *Nature.* 2000;403(6771):795–800.
23. Revollo JR, Grimm AA, Imai S. The NAD biosynthesis pathway mediated by nicotinamide phosphoribosyltransferase regulates Sir2 activity in mammalian cells. *J Biol Chem.* 2004;279(49):50754–50763.
24. Onyango P, Celic I, McCaffery JM, Boeke JD, Feinberg AP. SIRT3, a human SIR2 homologue, is an NAD-dependent deacetylase localized to mitochondria. *Proc Natl Acad Sci U S A.* 2002;99(21):13653–13658.
25. Scher MB, Vaquero A, Reinberg D. SirT3 is a nuclear NAD+-dependent histone deacetylase that translocates to the mitochondria upon cellular stress. *Genes Dev.* 2007;21(8):920–928.
26. Schwer B, North BJ, Frye RA, Ott M, Verdin E. The human silent information regulator (Sir)2 homologue hSIRT3 is a mitochondrial nicotinamide adenine dinucleotide-dependent deacetylase. *J Cell Biol.* 2002;158(4):647–657.
27. Shi T, Wang F, Stieren E, Tong Q. SIRT3, a mitochondrial sirtuin deacetylase, regulates mitochondrial function and thermogenesis in brown adipocytes. *J Biol Chem.* 2005;280(14):13560–13567.
28. Hallows WC, Lee S, Denu JM. Sirtuins deacetylate and activate mammalian acetyl-CoA synthetases. *Proc Natl Acad Sci U S A.* 2006;103(27):10230–10235.
29. Schwer B, Bunkenborg J, Verdin RO, Andersen JS, Verdin E. Reversible lysine acetylation controls the activity of the mitochondrial enzyme acetyl-CoA synthetase 2. *Proc Natl Acad Sci U S A.* 2006;103(27):10224–10229.
30. Ahn BH, et al. A role for the mitochondrial deacetylase Sirt3 in regulating energy homeostasis. *Proc Natl Acad Sci U S A.* 2008;105(38):14447–14452.
31. Lombard DB, et al. Mammalian Sir2 homolog SIRT3 regulates global mitochondrial lysine acetylation. *Mol Cell Biol.* 2007;27(24):8807–8814.
32. Tsai FC, Gardner DK. Nicotinamide, a component of complex culture media, inhibits mouse embryo development in vitro and reduces subsequent developmental potential after transfer. *Fertil Steril.* 1994;61(2):376–382.
33. Fato R, et al. Differential effects of mitochondrial Complex I inhibitors on production of reactive oxygen species. *Biochim Biophys Acta.* 2009; 1787(5):384–392.
34. Dumollard R, Duchen M, Carroll J. The role of mitochondrial function in the oocyte and embryo. *Curr Top Dev Biol.* 2007;77:21–49.
35. Kruse JP, Gu W. Modes of p53 regulation. *Cell.* 2009;137(4):609–622.
36. Vousden KH, Ryan KM. p53 and metabolism. *Nat Rev Cancer.* 2009;9(10):691–700.
37. Menendez D, Inga A, Resnick MA. The expanding universe of p53 targets. *Nat Rev Cancer.* 2009;9(10):724–737.
38. Riley T, Sontag E, Chen P, Levine A. Transcriptional control of human p53-regulated genes. *Nat Rev Mol Cell Biol.* 2008;9(5):402–412.
39. Han MK, Song EK, Guo Y, Ou X, Mantel C, Broxmeyer HE. SIRT1 regulates apoptosis and Nanog expression in mouse embryonic stem cells by controlling p53 subcellular localization. *Cell Stem Cell.* 2008;2(3):241–251.
40. Lin T, et al. p53 induces differentiation of mouse embryonic stem cells by suppressing Nanog expression. *Nat Cell Biol.* 2005;7(2):165–171.
41. Sundaresan NR, Samant SA, Pillai VB, Rajamohan SB, Gupta MP. SIRT3 is a stress-responsive deacetylase in cardiomyocytes that protects cells from stress-mediated cell death by deacetylation of Ku70. *Mol Cell Biol.* 2008;28(20):6384–6401.
42. Wallace DC, Fan W. The pathophysiology of mitochondrial disease as modeled in the mouse. *Genes Dev.* 2009;23(15):1714–1736.
43. Jacobs KM, et al. SIRT3 interacts with the daf-16 homolog FOXO3a in the mitochondria, as well as increases FOXO3a dependent gene expression. *Int J Biol Sci.* 2008;4(5):291–299.
44. Turrens JF. Mitochondrial formation of reactive oxygen species. *J Physiol.* 2003;552(pt 2):335–344.
45. Sundaresan NR, Gupta M, Kim G, Rajamohan SB, Isbatan A, Gupta MP. Sirt3 blocks the cardiac hypertrophic response by augmenting Foxo3a-dependent antioxidant defense mechanisms in mice. *J Clin Invest.* 2009;119(9):2758–2771.
46. Jin XL, Chandrakanthan V, Morgan HD, O'Neill C. Preimplantation embryo development in the mouse requires the latency of TRP53 expression,

which is induced by a ligand-activated PI3 kinase/AKT/MDM2-mediated signaling pathway. *Biol Reprod.* 2009;81(1):234–242.
47. Jones SN, Roe AE, Donehower LA, Bradley A. Rescue of embryonic lethality in Mdm2-deficient mice by absence of p53. *Nature.* 1995;378(6553):206–208.
48. Montes de Oca Luna R, Wagner DS, Lozano G. Rescue of early embryonic lethality in mdm2-deficient mice by deletion of p53. *Nature.* 1995; 378(6553):203–206.
49. Karawajew L, Rhein P, Czerwony G, Ludwig WD. Stress-induced activation of the p53 tumor suppressor in leukemia cells and normal lymphocytes requires mitochondrial activity and reactive oxygen species. *Blood.* 2005;105(12):4767–4775.
50. Favetta LA, Robert C, St John EJ, Betts DH, King WA. p66shc, but not p53, is involved in early arrest of in vitro-produced bovine embryos. *Mol Hum Reprod.* 2004;10(6):383–392.
51. Velez-Pardo C, Morales AT, Del Rio MJ, Olivera-Angel M. Endogenously generated hydrogen peroxide induces apoptosis via mitochondrial damage independent of NF-kappaB and p53 activation in bovine embryos. *Theriogenology.* 2007;67(7):1285–1296.
52. Jones RG, et al. AMP-activated protein kinase induces a p53-dependent metabolic checkpoint. *Mol Cell.* 2005;18(3):283–293.
53. Okoshi R, et al. Activation of AMP-activated protein kinase induces p53-dependent apoptotic cell death in response to energetic stress. *J Biol Chem.* 2008;283(7):3979–3987.
54. Luo J, et al. Negative control of p53 by Sir2alpha promotes cell survival under stress. *Cell.* 2001; 107(2):137–148.
55. Vaziri H, et al. hSIR2(SIRT1) functions as an NAD-dependent p53 deacetylase. *Cell.* 2001; 107(2):149–159.
56. Ito A, et al. p300/CBP-mediated p53 acetylation is commonly induced by p53-activating agents and inhibited by MDM2. *EMBO J.* 2001; 20(6):1331–1340.
57. Marchenko ND, Wolff S, Erster S, Becker K, Moll UM. Monoubiquitylation promotes mitochondrial p53 translocation. *EMBO J.* 2007;26(4):923–934.
58. Aida T, Oda S, Awaji T, Yoshida K, Miyazaki S. Expression of a green fluorescent protein variant in mouse oocytes by injection of RNA with an added long poly(A) tail. *Mol Hum Reprod.* 2001;7(11):1039–1046.

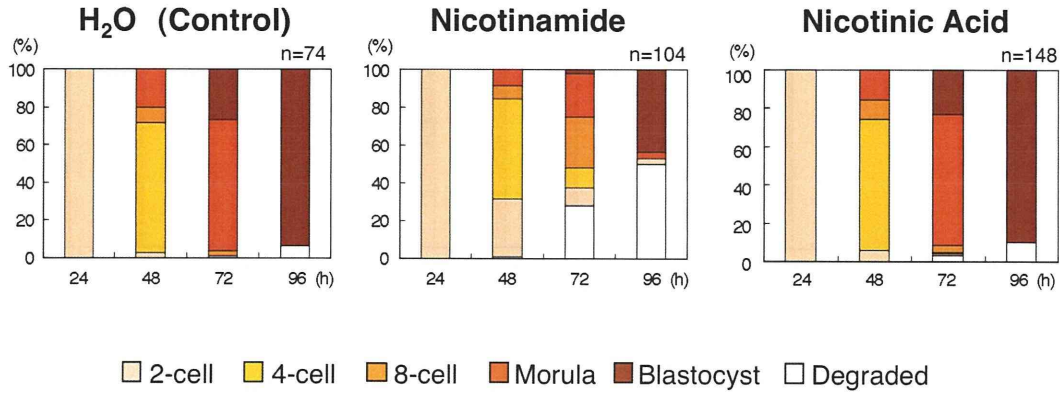

Figure S1

Effects of nicotinamide and nicotinic acid on development of in vitro fertilized and cultured embryos. Each column shows a breakdown of developmental stages at the indicated time after fertilization. Nicotinamide, but not nicotinic acid, caused developmental delay or arrest from the second cleavage.

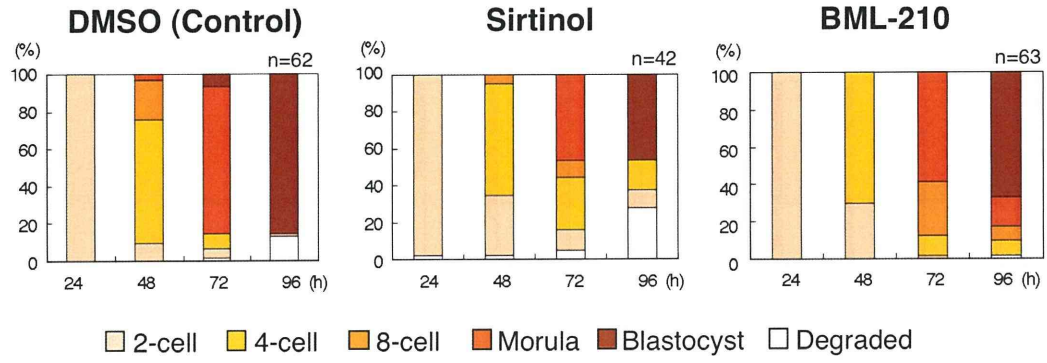

Figure S2

Effects of sirtinol and BML-210 on development of in vitro fertilized and cultured embryos. Each column shows a breakdown of developmental stages at the indicated time after fertilization. Both sirtuin inhibitors caused developmental delay or arrest from the second cleavage.

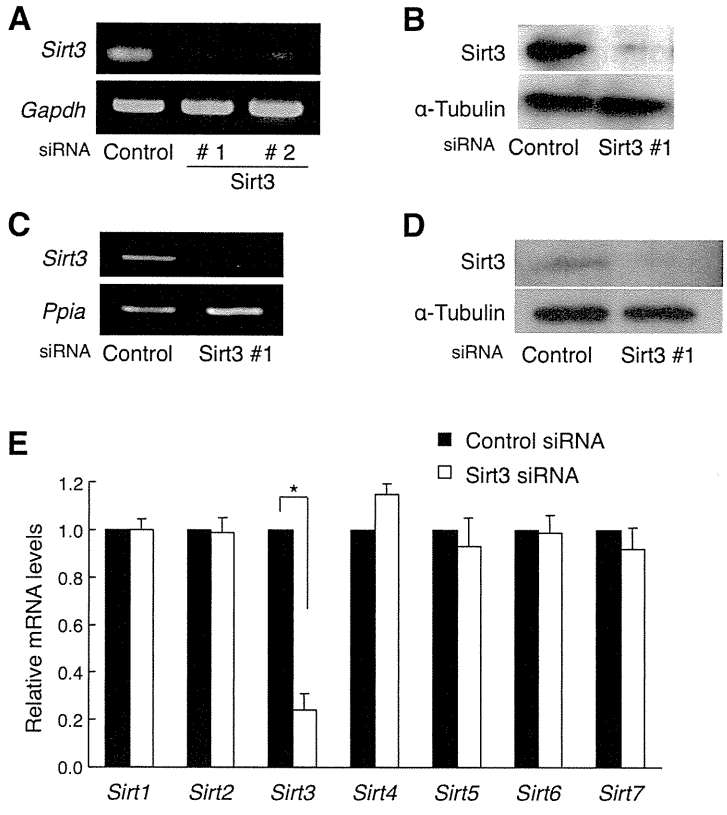

Figure S3

RNAi-mediated Sirt3 knockdown. Stealth RNAs targeting two different regions of Sirt3 transcript (#1 and #2 for nucleotides 355 to 379 and 386 to 410, respectively) downregulated Sirt3 mRNA and protein levels. (**A**) NIH-3T3 cells were transfected with Sirt3-targeted or control siRNAs. 48 hours after transfection, the effects of siRNAs were evaluated by RT-PCR analysis for Sirt3 mRNA expression. (**B**) Western blotting analysis for Sirt3 protein in NIH 3T3 cells. The decrease of Sirt3 protein by siRNA#1 transfection was detected. Blotting for α-tubulin served as an internal control. (**C**) Pronuclear stage embryos were injected with Sirt3 or control siRNAs. The effects of siRNAs were evaluated at 8-cell stage by RT-PCR analysis for Sirt3 mRNA expression. . (**D**) Western blotting analysis for Sirt3 protein in embryos. The decrease of Sirt3 protein by siRNA#1 transfection was detected at 8-cell stage. Blotting for α-tubulin served as an internal control. (**E**) Effects of Sirt3 knockdown on sirtuin gene expression. Real-time RT-PCR analysis was performed 24 h after siRNA injection. Sirt3 siRNA did not affect sirtuin gene expression except for *Sirt3* itself. Data are derived from 3 independent experiments. Statistical assessments were performed by applying Mann-Whitney U test. *$p<0.05$.

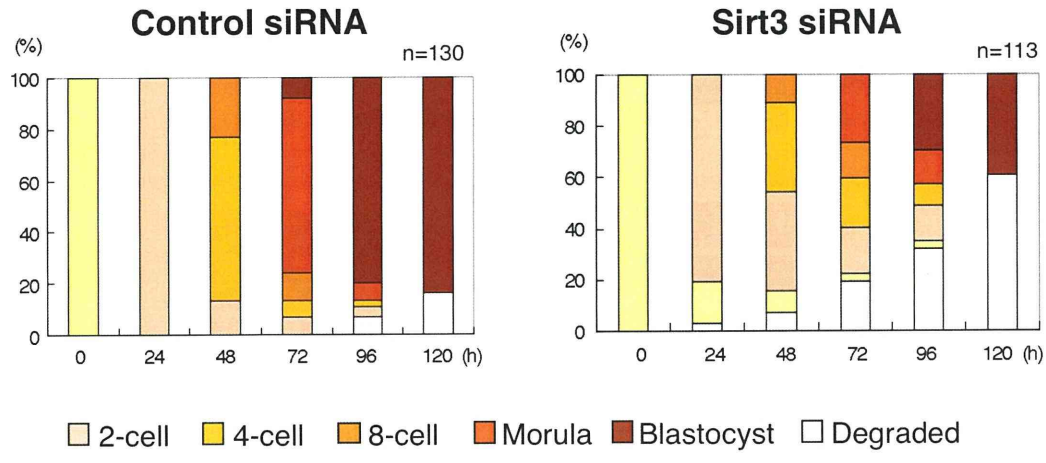

Figure S4

Effects of Sirt3 siRNA injection on development of in vitro fertilized and cultured embryos. Each column shows a breakdown of developmental stages at the indicated time after fertilization. siRNA-mediated Sirt3 knockdown caused developmental delay or arrest from the second cleavage.

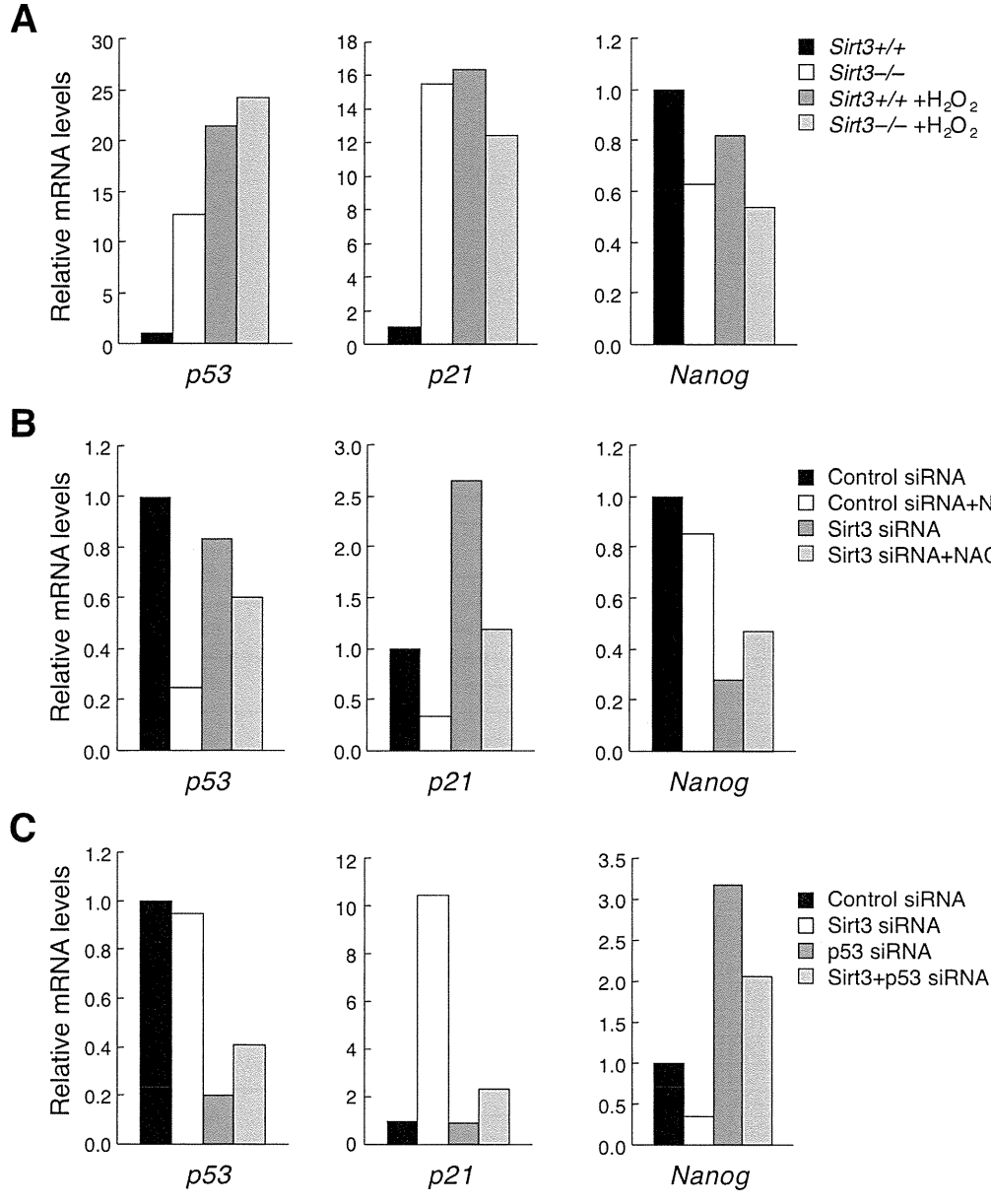

Figure S5

Quantification of *p53*, *p21* and *Nanog* mRNA levels in Sirt3-deficient preimplantation embryos in various conditions. (**A**) Effects of treatment with H_2O_2 on *p53*, *p21* and *Nanog* expression in wild-type and *Sirt3–/–* embryos. (**B**) Effects of Sirt3 knockdown and treatment with NAC *p53*, *p21* and *Nanog* expression. (**C**) Effects of p53 knockdown on Sirt3 siRNA-induced changes in *p21* and *Nanog* expression. Data are means of 2 to 4 independent experiments, examining more than 20 embryos for each experiment.

Supplemental Table S1
Primers and reaction conditions for conventional RT–PCR.

Gene	Primers		Product size (bp)	Annealing (°C)
Sirt1	forward	5'-CCTTGGAGACTGCGATGTTA-3'	158	58
	reverse	5'-GTGTTGGTGGCAACTCTGAT-3'		
Sirt2	forward	5'-GCAGTGTCAGAGCGTGGTAA-3'	170	60
	reverse	5'-CTAGTGGTGCCTTGCTGATG-3'		
Sirt3	forward	5'-TACAGGCCCAATGTCACTCA-3'	168	63
	reverse	5'-ACAGACCGTGCATGTAGCTG-3'		
Sirt4	forward	5'-CGCTGCTCAAGATCCCTAAG-3'	179	60
	reverse	5'-GCGACACAGCTACTCCATCA-3'		
Sirt5	forward	5'-GACTCAAGACGCCAGAATCC-3'	179	60
	reverse	5'-CAGAGGATGTTCCCACCACT-3'		
Sirt6	forward	5'-CTGGTCTGGAACTCACTGCT-3'	238	60
	reverse	5'-CGGGTGTGATTGGTAGAGAG-3'		
Sirt7	forward	5'-GGCACTTGGTTGTCTACACG-3'	160	60
	reverse	5'-GTGATGCTCATGTGGGTGAG-3'		
p53	forward	5'-GACCGCCGTACAGAAGAAGA-3'	159	63
	reverse	5'-GCGGATCTTGAGGGTGAAATA-3'		
p21	forward	5'-GTACTTCCTCTGCCCTGCT-3'	171	60
	reverse	5'-TGCGCTTGGAGTGATAGA-3'		
Nanog	forward	5'-AGGGTCTGCTACTGAGATGCT-3'	364	60
	reverse	5'-CAACACCTGGTTTTTCTGCCACCG-3'		
Ppia	forward	5'-CGCGTCTCCTTCGAGCTGTTTG-3'	150	64
	reverse	5'-TGTAAAGTCACCACCCTGGCACAT-3'		
Gapdh	forward	5'-GGTGTGAACCACGAGAAATAT-3'	334	61
	reverse	5'-AGATCCACGACGGACACATT-3'		

Supplemental Table S2
Primers and reaction conditions for real-time RT-PCR.

Gene	Primers		Product size (bp)	Annealing (°C)
Sirt1	forward	5'-CCTTGGAGACTGCGATGTTA-3'	158	63
	reverse	5'-GTGTTGGTGGCAACTCTGAT-3'		
Sirt2	forward	5'-GCAGTGTCAGAGCGTGGTAA-3'	170	63
	reverse	5'-CTAGTGGTGCCTTGCTGATG-3'		
Sirt3	forward	5'-CTGACTTCGCTTTGGCAGAT-3'	206	63
	reverse	5'-GTCCACCAGCCTTTCCACAC-3'		
Sirt4	forward	5'-CGCTGCTCAAGATCCCTAAG-3'	179	63
	reverse	5'-GCGACACAGCTACTCCATCA-3'		
Sirt5	forward	5'-AGCCAGAGACTCAAGACGCCA-3'	151	63
	reverse	5'-AGGGCGAGCTCTCTGTCCACC-3'		
Sirt6	forward	5'-TCGGGCCTGTAGAGGGGAGC-3'	174	63
	reverse	5'-CGGCGCTTAGTGGCAAGGGG-3'		
Sirt7	forward	5'-GGCACTTGGTTGTCTACACG-3'	121	60
	reverse	5'-AGGTCGGCAGCACTCACAGG-3'		
p53	forward	5'-GACCGCCGTACAGAAGAAGA-3'	159	63
	reverse	5'-GCGGATCTTGAGGGTGAAATA-3'		
p21	forward	5'-GTACTTCCTCTGCCCTGCT-3'	171	60
	reverse	5'-TGCGCTTGGAGTGATAGA-3'		
Nanog	forward	5'-GGAAGCAGAAGATGCGGACT-3'	177	60
	reverse	5'-ACCGCTTGCACTTCATCCTT-3'		
Ppia	forward	5'-CAGGTCCTGGCATCTTGTCC-3'	239	63
	reverse	5'-ATGCCCGCAAGTCAAAAGAA-3'		

Development 137, 3823-3833 (2010) doi:10.1242/dev.054015

Endothelin receptor type A expression defines a distinct cardiac subdomain within the heart field and is later implicated in chamber myocardium formation

Rieko Asai[1], Yukiko Kurihara[1], Kou Fujisawa[1], Takahiro Sato[1], Yumiko Kawamura[1], Hiroki Kokubo[2,3], Kazuo Tonami[1], Koichi Nishiyama[1], Yasunobu Uchijima[1], Sachiko Miyagawa-Tomita[4] and Hiroki Kurihara[1,*]

SUMMARY

The avian and mammalian heart originates from two distinct embryonic regions: an early differentiating first heart field and a dorsomedially located second heart field. It remains largely unknown when and how these subdivisions of the heart field divide into regions with different fates. Here, we identify in the mouse a subpopulation of the first (crescent-forming) field marked by endothelin receptor type A (*Ednra*) gene expression, which contributes to chamber myocardium through a unique type of cell behavior. *Ednra-lacZ/EGFP*-expressing cells arise in the ventrocaudal inflow region of the early linear heart tube, converge to the midline, move anteriorly along the outer curvature and give rise to chamber myocardium mainly of the left ventricle and both atria. This movement was confirmed by fluorescent dye-labeling and transplantation experiments. The *Ednra-lacZ/EGFP*-expressing subpopulation is characterized by the presence of *Tbx5*-expressing cells. *Ednra*-null embryonic hearts often demonstrate hypoplasia of the ventricular wall, low mitotic activity and decreased *Tbx5* expression with reciprocal expansion of *Tbx2* expression. Conversely, endothelin 1 stimulates ERK phosphorylation and *Tbx5* expression in the early embryonic heart. These results indicate that early *Ednra* expression defines a subdomain of the first heart field contributing to chamber formation, in which endothelin 1/Ednra signaling is involved. The present finding provides an insight into how subpopulations within the crescent-forming (first) heart field contribute to the coordination of heart morphogenesis through spatiotemporally defined cell movements.

KEY WORDS: Cardiac development, Heart fields, Endothelin, Mouse

INTRODUCTION

The heart is the first functioning organ to develop during embryogenesis. Different sources of cell populations from the cardiogenic mesoderm and the cardiac neural crest coordinately contribute to the formation of elaborate cardiac structures, including the four specialized chambers, the valves and supporting tissues, and the conduction system (Buckingham et al., 2005; Cai et al., 2008; Kirby, 2007; Zhou et al., 2008). Myocardial progenitor cells first appear bilaterally in the anterior splanchnic mesoderm and move towards the midline to form the cardiac crescent and then the primary heart tube. Through subsequent growth by accretion of cells at the poles from a newly identified progenitor population called the second heart field (Cai et al., 2003; Galli et al., 2008; Kelly et al., 2001; Mjaatvedt et al., 2001; Waldo et al., 2001), the heart tube loops and in subsequent steps is sculpted into a four-chambered heart in mammals and birds (Abu-Issa and Kirby, 2007; Buckingham et al., 2005; Laugwitz et al., 2008).

[1]Department of Physiological Chemistry and Metabolism, Graduate School of Medicine, The University of Tokyo, 7-3-1 Hongo, Bunkyo-ku, Tokyo 113-0033, Japan. [2]Division of Mammalian Development, National Institute of Genetics, 1111 Yata, Mishima Shizuoka 411-8540, Japan. [3]Department of Genetics, The Graduate University for Advanced studies, 1111 Yata, Mishima Shizuoka 411-8540, Japan. [4]Division of Cardiovascular Development and Differentiation, Medical Research Institute, Department of Pediatric Cardiology, Tokyo Women's Medical University, 8-1 Kawada-cho, Shinjuku-ku, Tokyo 162-8666, Japan.

*Author for correspondence (kuri-tky@umin.ac.jp)

Accepted 3 September 2010

The distinction between these two heart fields is further supported by retrospective clonal analysis using recombinant *lacZ* labeling (Meilhac et al., 2004). This analysis, in embryonic day (E) 8.5 mouse embryos, revealed two distinct cell lineages with different patterns of regionalization in the heart tube. The first lineage contributed to all left ventricular myocardium, some of the right ventricular myocardium, the atrioventricular canal and both atria. The second lineage contributed to the outflow tract and all other myocardial regions except for the left ventricle. Notably, the second lineage appears to correspond roughly to the second heart field marked by *Islet1* (*Isl1* – Mouse Genome Informatics) expression in terms of regional contribution (Cai et al., 2003; Galli et al., 2008). The clonal analysis also revealed that the two cell lineages segregate from a common progenitor around the time of gastrulation (Meilhac et al., 2004). Based on these findings, the first lineage is postulated to segregate first from the common progenitor pool to form the heart tube (Buckingham et al., 2005).

Following their segregation, the heart fields are probably further regionalized and diversified into various cell types. However, it remains largely unknown when and how different subpopulations arise within these heart-forming fields and how they interact with each other to coordinate heart morphogenesis.

Endothelin 1 (Edn1)/endothelin receptor type A (Ednra) signaling is known to be involved in cardiovascular and craniofacial development (Clouthier et al., 1998; Kurihara et al., 1994; Ozeki et al., 2004; Sato et al., 2008a; Sato et al., 2008b). Mice deficient in Edn1/Ednra signaling exhibit aortic arch malformation and outflow anomalies, which are attributed to cardiac neural crest defects (Kurihara et al., 1995; Yanagisawa et al., 1998). Correspondingly, *Ednra* is expressed in cranial and

cardiac neural crest-derived mesenchymal cells (Clouthier et al., 1998; Kurihara et al., 1995; Maemura et al., 1996; Yanagisawa et al., 1998).

Recently, we established mice in which *lacZ* (which encodes β-galactosidase) and *EGFP* (which encodes enhanced green fluorescent protein) were introduced into the *Ednra* locus to recapitulate its endogenous expression (Sato et al., 2008a). Consequently, *lacZ/EGFP* expression emerged in the developing heart with a characteristic pattern. We then focused on this expression, expecting that it might lead to the identification of a novel myocardial subpopulation. Here, we demonstrate that early *Ednra-lacZ/EGFP* expression marks a subpopulation of the heart field with distinct regional identity. *Ednra-lacZ/EGFP*-positive cells are first localized in the ventral inflow region, move anteriorly along the outer curvature following the formation of the heart tube, and give rise to chamber myocardium. Dye-labeling and transplantation experiments confirmed this movement and contribution to chamber formation. We also observed developmental abnormalities in *Ednra*-null embryonic hearts, indicating the involvement of Edn1 as a mitotic factor in early cardiac development.

MATERIALS AND METHODS

Mice

$Ednra^{lacZ+}$ (*lacZ* knock-in) mice have been described previously (Sato et al., 2008a). To generate mice carrying the $Ednra^{EGFP}$ (*EGFP* knock-in) allele, we performed Cre recombinase-mediated cassette exchange (RMCE) on $Ednra^{neo+}$ embryonic stem (ES) cells in which an exchangeable floxed site was introduced into the *Ednra* locus as described previously (Sato et al., 2008a) (see Fig. S1 in the supplementary material). Briefly, the EGFP cassette excised from the pEGFP-N3 expression vector (Clontech) was introduced into the knock-in vector p66-2272 containing multiple cloning sites between *lox66* and *lox2272* (Araki et al., 2002). The resultant plasmids were transfected into $Ednra^{neo+}$ ES cells with AxCANCre recombinant adenovirus expressing the recombinase Cre tagged with a nuclear localization signal under the control of the CAG promoter (Kanegae et al., 1995). Targeted ES clones were injected into ICR blastocysts to generate germline chimeras that were then crossed with ICR females. Mice were housed in an environmentally controlled room at 23±2°C, with a relative humidity of 50-60% and under a 12-hour light:12-hour dark cycle. Genotypes were determined by PCR on tail-tip or amnion DNA using primers specific for RMCE-mediated recombination. Embryonic ages were determined by timed mating with the day of the plug being E0.5. The number of somites was also used to estimate developmental stages from E7.8 to E8.5. All animal experiments were reviewed and approved by the University of Tokyo Animal Care and Use Committee.

β-Galactosidase staining

lacZ expression was detected by staining with X-Gal (5-bromo-4-chloro-3-indolyl β-D-galactoside) for β-galactosidase activity. Whole-mount and section staining were performed as described previously (Nagy et al., 2003).

Immunohistochemistry

Embryo cryosections (12 μm) were immunostained using the following antibodies: rat monoclonal anti-GFP (Nacalai Tesque, Kyoto, Japan; 1:200), rabbit anti-GFP (Medical and Biological Laboratories, Nagoya, Japan; 1:250), rabbit anti-Nkx2.5 (Santa Cruz, 1:250), mouse monoclonal anti-Isl1 (39.5D5; Developmental Studies Hybridoma Bank; 1:100), mouse monoclonal anti-myosin heavy chain (MHC) (MF20-c; Developmental Studies Hybridoma Bank; 1:100), rabbit anti-desmin (Progen Biotechnik, Heidelberg, Germany; 1:200), mouse monoclonal phycoerythrin (PE)-conjugated anti-CD31 (BD Pharmingen; 1:200), mouse monoclonal anti-BrdU (Calbiochem; 1:20) and rabbit anti-phosphohistone H3 (pHH3) (Ser10) (Upstate Biotechnology; 1:250). Signals were visualized with horseradish peroxidase- or FITC-conjugated secondary antibodies specific for the appropriate species. Some sections were treated with biotin-conjugated secondary antibodies and visualized using the VECTASTAIN ABC System (Vector Laboratories), streptavidin-FITC (Dako; 1:200) or streptavidin-TRITC (1:200, Beckman Coulter). Nuclei were visualized with TO-PRO-3 (Molecular Probes).

In situ hybridization

Whole-mount in situ hybridization was performed as described previously (Wilkinson, 1992). Sections (12 μm) were prepared from frozen embryos. Treatment for in situ hybridization was as described previously with minor modifications (Ishii et al., 1997). The *Ednra*, *Cited1*, *Tbx2* and *Bmp2* probes have been described previously (Kokubo et al., 2007; Sato et al., 2008a). Probes for *Nkx2.5* (*Nkx2-5* – Mouse Genome Informatics), *Mlc2a* (*Myl7* – Mouse Genome Informatics) and *Isl1* (GenBank accession numbers: NM_008700, NM_021459 and NM_022879, respectively) were prepared using RT-PCR. The *Tbx5* probe was obtained from V. E. Papaioannou (Chapman et al., 1996; Sato et al., 2008a). The *Cx40* (*Gja5* – Mouse Genome Informatics) probe was obtained from D. Gros (Delorme et al., 1997). The *ANF* (*Nppa* – Mouse Genome Informatics) probe was obtained from T. Watanabe (Koibuchi and Chin, 2007). The *Hand1* probe was from D. Srivastava (Srivastava et al., 1995).

Fluorescent dye labeling

Embryos from 6- or 7-somite stages were collected, transferred to DMEM/F12 containing 10% FCS, and injected with PKH67 (green) or PKH26 (red) fluorescent dyes (Sigma) using a needle drawn from glass capillary tubing in order to label cells in the *lacZ*- or *EGFP*-expressing or adjacent regions. Embryos were then placed in a 15-ml culture bottle containing 2 ml culture medium (50% rat serum plus 50% DMEM/F12) and rotated at 20 rpm at 37°C while being continuously supplied with a suitable concentration of O_2 (5 or 20%) and CO_2 (5%) balanced with N_2 for 30 hours. Labeled embryos were observed using a Leica MZFLIII stereomicroscope equipped with a Hamamatsu C4742-95 digital camera. Some embryos were fixed for X-gal staining. For whole-heart labeling, E8.25 (6- to 7-somite stage) embryos were incubated in DMEM/F12 with 1 μM SYTO16 (Molecular Probes), which stains the nuclei of live cells, at 37°C in 5% CO_2 for 30 minutes, and the heart tubes were excised.

Transplantation and explant culture experiment

Cardiac inflow tissues corresponding to the *Ednra-lacZ/EGFP*-positive region were excised from E8.25 (5- to 7-somite stage) embryos and transplanted into the same regions of recipient embryos (without removing their own inflow regions) using fine glass and tungsten needles. The *Ednra-EGFP*-positive tail regions were also transplanted as a control experiment. For transplantation of SYTO16-labeled cells, heart tubes were cut into three parts (outflow, ventricular and inflow regions) and were transplanted into the inflow regions of recipient embryos. Embryos were then placed in a collagen-coated 3.5-cm dish containing 500 μl α-MEM with 10% horse serum at 37°C in 5% CO_2 balanced with N_2 for 24 hours. Following culture, embryos were observed under a fluorescence microscope or fixed in 4% paraformaldehyde and subjected to immunostaining. For explant culture, dissected SYO16-labeled tissues were placed onto collagen-coated dishes and were incubated in α-MEM with 10% horse serum at 37°C in 5% CO_2 for 24 hours.

BrdU labeling

Pregnant female mice at E9.5 were injected intraperitoneally with bromodeoxyuridine (BrdU; 0.2 mg/g body weight; Sigma). After 1 hour of BrdU exposure, embryos were harvested on ice-cold PBS to stop BrdU incorporation and were fixed in 4% paraformaldehyde for 1 hour. Cryosections were treated with 2 M HCl and subjected to immunostaining with anti-BrdU antibody. For each sample, two sequential transverse sections through the widest region of the left and right ventricles were taken and BrdU-positive nuclei were counted in the compact, trabecular and endocardial layers of the ventricular wall. The sections were then counterstained with Hematoxylin to visualize nuclei and the total of

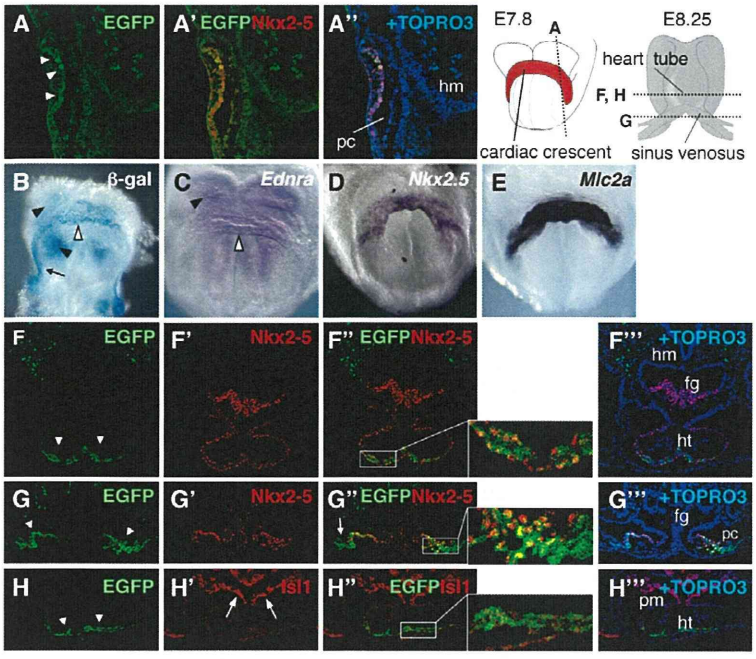

Fig. 1. *Ednra-lacZ/EGFP* expression in early developing hearts at the 1- to 4-somite stages. (**A-A″**) Sagittal sections of a 1-somite stage *Ednra-EGFP* mouse embryo immunostained for EGFP (A; green) and Nkx2.5 (A′; red), merged with TO-PRO-3 staining for nuclei (A″; blue). EGFP-positive cells were detected within the Nkx2.5-positive heart-forming region (white arrowheads). (**B**) Ventral view of a 3-somite stage *Ednra-lacZ* embryo stained for β-galactosidase activity. *lacZ*-expressing cells were detected within the cardiac crescent (white arrowhead), non-cardiogenic mesoderm (arrow) and head mesenchyme behind the crescent (black arrowheads). (**C-E**) Whole-mount in situ hybridization for *Ednra* (C), *Nkx2.5* (D) and *Mlc2a* (E) on a 3-somite stage embryo. White and black arrowheads indicate *Ednra* expression in the cardiac crescent and head mesenchyme, respectively. (**F-H‴**) Transverse sections of 4-somite stage *Ednra-EGFP* embryos immunostained for EGFP (F,G,H,F″,G″,H″) and Nkx2.5 (F′,F″,G′,G″) or Isl1 (H′,H″) with TO-PRO-3 staining (F‴,G‴,H‴). The boxed regions in F″,G″,H″ are magnified in the panels to the right. EGFP-positive cells were detected within the Nkx2.5-positive heart tube (arrowheads) and Nkx2.5-negative lateral plate mesoderm (arrow in G″). EGFP expression did not overlap with Isl1 expression in the second heart field (arrows in H′). Planes of sections are indicated in the diagrams at the top. fg, foregut; hm, head mesenchyme; ht, heart tube; pc, pericardial coelom; pm, pharyngeal mesoderm.

number nuclei was counted in order to calculate the ratio of BrdU-positive to total nuclei. Statistical significance ($P<0.05$) was determined using the paired *t*-test. Data are presented as mean±s.e.m.

Phosphorylation of ERK

Hearts were collected from E9.5 wild-type, *Ednra*$^{+/EGFP}$ and *Ednra*$^{EGFP/EGFP}$ embryos and lysed with lysis buffer [50 mM Tris-HCl (pH 8.0), 150 mM NaCl, 1 mM EDTA, 1% Triton X-100, 0.1% SDS, 0.1% sodium deoxycholate, protease inhibitor cocktail (Roche), 1 mM sodium orthovanadate and 1 mM sodium fluoride]. The lysates were subjected to SDS-PAGE and immunoblotted using a mouse monoclonal antibody to phosphorylated ERK1/2 and a rabbit polyclonal antibody to total ERK1/2 (both Cell Signaling Technology). To evaluate the effect of Edn1, E9.5 wild-type hearts were incubated in serum-free DMEM with or without 10 μM BQ123 (a cyclic peptide) for 3 hours then stimulated with 100 nM Edn1 for 5 minutes at 37°C. To evaluate the effect of BQ123 on basal ERK phosphorylation, E9.5 wild-type hearts were incubated in DMEM containing 10% fetal calf serum with or without 10 μM BQ123 for 3 hours. Signal intensity was quantified with ImageJ software (NIH). One-way analysis of variance (ANOVA) with Tukey's test was applied for comparisons of phosphorylated ERK levels among genotypes.

Conventional RT-PCR

Hearts were collected from E8.25 and E9.5 embryos and sorted into EGFP-positive and EGFP-negative cells using a FACS VantageSE (BD Biosciences). Total RNA was extracted from sorted fractions with the use of Isogen (Nippon Gene, Tokyo, Japan), and 1 μg samples were then reverse-transcribed using ReverTra Ace (Toyobo, Osaka, Japan) with oligo(dT) primer (Takara Bio, Shiga, Japan). The resulting cDNAs were amplified with Taq polymerase (Takara Bio) in a thermocycler. The sequences of the forward and reverse primers as well as the amplicon lengths are listed in Table S1 in the supplementary material. Custom primers were designed using Primer-BLAST online software (http://www.ncbi.nlm.nih.gov/tools/primer-blast/). Thermal cycling was performed for 25-30 cycles to maintain PCR conditions within the linear range of amplification before saturation was reached. Each cycle consisted of 30 seconds of denaturation at 94°C, 30 seconds of annealing at each annealing temperature (see Table S1 in the supplementary material) and 30 seconds of extension at 72°C. Glyceraldehyde-3-phosphate dehydrogenase (*Gapdh*) was used as an internal control.

Quantitative real-time RT-PCR

Left ventricles were isolated from E9.5 embryos. To evaluate the effect of Edn1, isolated ventricles were cultured in DMEM plus 5% fetal calf serum with or without 100 nM Edn1 for 24 hours. Total RNA was extracted from a pool of seven samples for each genotype or culture condition. Quantification of the amount of each mRNA was performed by real-time RT-PCR analyses using a LightCycler (Roche) and Real-Time PCR Premix with SYBR Green (RBC Bioscience) following the manufacturer's protocol. The primers and reaction conditions are shown in Table S1 in the supplementary material. Thermal cycling was performed for 47 cycles after incubation at 96°C for 10 minutes in at least three separate runs. Each cycle consisted of 10 seconds of denaturation at 95°C, 10 seconds of annealing at each annealing temperature (see Table S1 in the supplementary material) and 11 seconds of extension at 72°C. The second-derivative maximum method was adopted to determine the crossing points automatically for individual samples, and relative amounts of mRNA were calculated based on the crossing-point analysis. Hypoxanthine phosphoribosyltransferase (*Hprt*) was used as an internal control. The result was expressed as a fold change relative to the control. The Mann-Whitney *U*-test was applied for comparisons of relative mRNA levels between genotypes or culture conditions.

RESULTS

Ednra-lacZ/EGFP expression defines a distinct subdomain within the cardiac crescent

We characterized marker gene expression in the embryonic heart of *Ednra*$^{lacZ/+}$ and *Ednra*$^{EGFP/+}$ mice. *Ednra-lacZ/EGFP*-positive cells were first detected in the crescent-forming cardiogenic mesoderm around the 1-somite stage (~E7.8) (Fig. 1A-A″). At the 1- to 3/4-somite stages (E7.8~E8.0), *Ednra-lacZ* signals coincided with detection of endogenous expression of *Ednra* (Fig. 1B,C) and were colocalized with *Nkx2.5* and *Mlc2a* (Fig. 1A′,A″,D,E). Double immunostaining on sections revealed that *Ednra-EGFP* expression overlapped with *Nkx2.5* expression in the ventral region of the heart tube (Fig. 1F-F″). In the caudal region, *Ednra-lacZ/EGFP* expression extended to the *Nkx2.5*-negative lateral plate mesoderm (Fig. 1B,G-G″) and to the extra-embryonic mesoderm of the amnion along the border with the embryonic

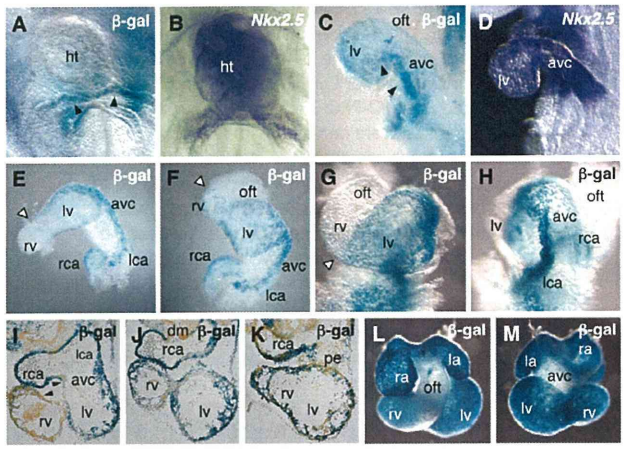

Fig. 2. β-Galactosidase staining and in situ hybridization for *Nkx2.5* on *Ednra-lacZ* hearts. (**A-D**) Hearts at 6/7- (A,B; ventral views) and 9/10- (C,D; left lateral views) somite stages, stained for β-galactosidase activity (A,C) or *Nkx2.5* expression (B,D). β-Galactosidase activity is most intense in the inflow region (arrowheads in A) and then extends towards the atrioventricular canal and left ventricle (arrowheads in C). (**E-H**) Dissected hearts at the 10- (E,F) and 13- (G,H) somite stages, stained for β-galactosidase activity and viewed from the inferior (E), ventral (F,G) and left-dorsal (H) sides. White arrowheads indicate boundaries of β-galactosidase expression. (**I-K**) Transverse sections of E9.5 *Ednra-lacZ* hearts stained for β-galactosidase activity. Sections are counterstained with Orange G. β-Galactosidase-positive cells contribute to all four chambers, but not to the atrioventricular canal and inner curvature. Arrowheads indicate expression boundaries along the inner curvature. Dorsal mesocardium and proepicardium were also negative for β-galactosidase activity. (**L**,**M**) Ventral (L) and dorsal (M) views of an E10.5 heart stained for β-galactosidase activity. avc, atrioventricular canal; dm, dorsal mesocardium; ht, heart tube; l/r(c)a, left/right (common) atrium; l/rv, left/right ventricle; oft, outflow tract; pe, proepicardium.

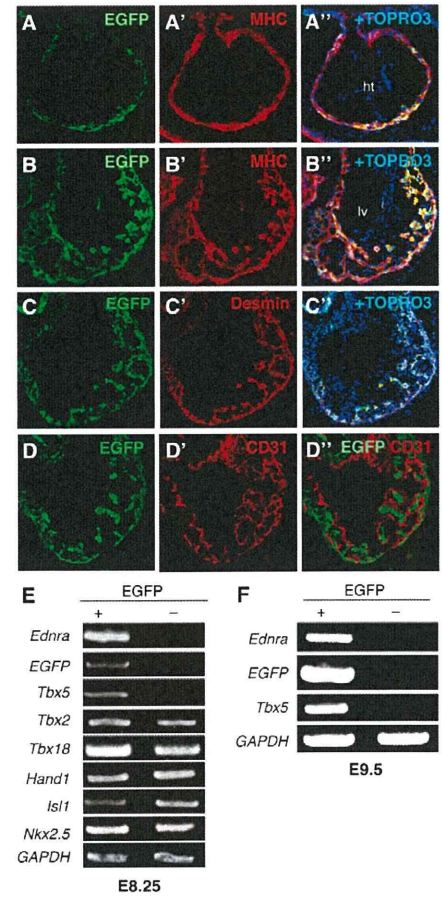

Fig. 3. Characterization of *Ednra-lacZ/EGFP*-expressing cells. (**A-D''**) Co-immunostaining for EGFP and cardiac markers in early *Ednra-EGFP* hearts. Transverse sections of E8.25 (7-somite stage; A-A'') and E9.5 (B-D'') *Ednra-EGFP* embryos immunostained for EGFP (A-D,D'') and myosin heavy chain (MHC; A',B'), desmin (C') or CD31 (D',D'') with TO-PRO-3 staining (A'',B'',C''). ht, heart tube; lv, left ventricle. (**E**,**F**) RT-PCR analysis of *Ednra-EGFP*-positive and -negative cells from E8.25 (E) and E9.5 (F) hearts.

body. In contrast with its colocalization with *Nkx2.5*, *EGFP* expression never overlapped with *Isl1* expression, which marks the second heart field located behind the forming heart tube at this stage (Cai et al., 2003) (Fig. 1H-H''). These findings indicate that the *Ednra-lacZ/EGFP*-expressing cells might represent a myocardial subdomain within the first heart field.

Ednra-lacZ/EGFP-positive cells contribute to the chamber-forming myocardium

During linear tube formation at the 6/7-somite stage (~E8.25), *Ednra-lacZ* expression was largely confined to the caudal inflow region corresponding to the venous pole (Fig. 2A,B). Subsequently, *Ednra-lacZ* expression was extended to the left lateral wall of the looping heart, forming an apparent trajectory along the outer curvature (Fig. 2C,D). At the 10- to 13-somite stage (~E8.5), β-galactosidase-positive cells were distributed from the venous pole to the left ventricle through a narrow region within the left lateral wall of the atrioventricular canal and atria (Fig. 2E-H). By contrast, the dorsal side of the heart, along the inner curvature and the outflow tract, lacked β-galactosidase expression (Fig. 2E-H). In the right ventricle, only the caudal (posterior) region was populated by β-galactosidase-positive cells (Fig. 2F,G). These patterns were almost identical to the endogenous *Ednra* expression revealed by in situ hybridization (see Fig. S2 in the supplementary material). At E9.5, β-galactosidase-positive cells were distributed in the common atrium, left ventricle and a posterior part of the right ventricle (Fig. 2I-K). By contrast, the trabeculation-free region in the inner curvature, dorsal mesocardium and proepicardium lacked β-galactosidase expression (Fig. 2I-K). At E10.5, β-galactosidase was widely expressed in the four chambers, whereas the atrioventricular canal and outflow tract were mostly negative (Fig. 2L,M).

To confirm that *Ednra-lacZ/EGFP* expression marked the myocardial cell lineage, we examined myocardial marker expression. In the E8.25 heart tube and the E9.5 left ventricle, EGFP expression overlapped with myosin heavy chain expression (Fig. 3A,B). At E9.5, EGFP-expressing cells also expressed desmin (Fig. 3C), a marker for chamber-forming myocardium (Schaart et al., 1989). By contrast, EGFP expression did not overlap with CD31 expression, which marks endocardial cells (Fig. 3D). EGFP-expressing cells were further characterized by fluorescence-activated cell sorting (FACS) and RT-PCR. At E8.25 and E9.5, only EGFP-positive fractions expressed *Ednra* and *EGFP*. Remarkably, expression of *Tbx5*, a T-box transcription factor gene crucial for early heart development (Bruneau et al., 2001; Takeuchi et al.,

2003), was also only detected in EGFP-positive fractions (Fig. 3E,F). Section staining confirmed the presence of Tbx5-positive cells in the *Ednra-EGFP*-expressing region, particularly in the caudal inflow region (see Fig. S2 in the supplementary material). These results indicate that *Ednra-lacZ/EGFP* expression marks chamber-forming cardiomyocytes, including *Tbx5*-positive cells arising in the inflow region.

Dye injected into the ventral inflow region follows the subsequent distribution of the *Ednra-lacZ/EGFP*-positive subdomain

Extension of *Ednra-lacZ/EGFP* expression along the outer curvature raises the possibility that *Ednra-lacZ/EGFP*-expressing cells in the ventral inflow region move into the linear heart tube to give rise to chamber myocardium. However, it is also possible that *Ednra-lacZ/EGFP* expression is sequentially upregulated with different timing in cells already present in the heart tube. These possibilities are not mutually exclusive. To examine whether the upward cell movement contributes to the extension of *Ednra-lacZ/EGFP* expression, we injected PKH fluorescent dyes into the ventral inflow region and adjacent areas at the 6/7-somite stage and cultured the injected embryos for 30 hours. The injected areas, distribution patterns of labeled cells and summary of the results are shown in Fig. 4A. After 30 hours, labeled cells were found in the left lateral wall of the atrium and atrioventricular canal towards the left ventricle (I in Fig. 4A) in 13 out of 14 embryos in which dye was injected into the middle (a in Fig. 4A; n=6) or left (b in Fig. 4A; n=8) portion of the ventral inflow region (Fig. 4B-C′). Labeled cells were also found in the left ventricle in three embryos in which dye was injected into the middle region (Fig. 4B′). These results support the possibility of cell movement. Interestingly, five out of six embryos in which dye was injected into the right portion of the ventral inflow region (c in Fig. 4A) also had labeled cells in the contralateral left wall of the atrium and atrioventricular canal after 30 hours (Fig. 4D,D′). The one remaining embryo showed labeled cells in the future right atrium (Fig. 4E,E′). Thus, dye-injection experiments indicate that *lacZ/EGFP*-positive cells on both sides of the inflow region at the 6/7-somite stage contribute to the cell population extending to the left ventricle.

By contrast, only two out of 13 embryos in which dye was injected into the adjacent *lacZ/EGFP*-negative region revealed labeled cells in the atrial wall (Fig. 4A; d-g). In one of those embryos, labeled cells appeared in the left dorsocranial wall 30 hours after injection into the *lacZ/EGFP*-negative region dorsomedially adjacent to the left *lacZ/EGFP*-positive region (Fig. 4; f→III); in the other, labeled cells were detected in the right lateral wall after injection into the right *lacZ/EGFP*-negative region (Fig. 4; g→II). These distribution patterns are consistent with the previous report that cells in the right and left posterior second heart field contribute to the corresponding right and left wall of the atrium (Galli et al., 2008).

When transplanted, the *Ednra-lacZ/EGFP*-positive inflow region contributes to left ventricular and atrial myocardium

To confirm the movement from the ventral inflow region to the developing left ventricle and atrium, we transplanted, at E8.25 (5- to 7-somite stage), the *Ednra-lacZ/EGFP*-positive inflow region into the same region of wild-type embryos (Fig. 5A). After 24 hours, *Ednra-EGFP*-positive cells were detected in the left ventricle in five out of eight recipient embryos transplanted with the $Ednra^{EGFP+}$ inflow region (Fig. 5B-B″). By contrast, no EGFP signals were

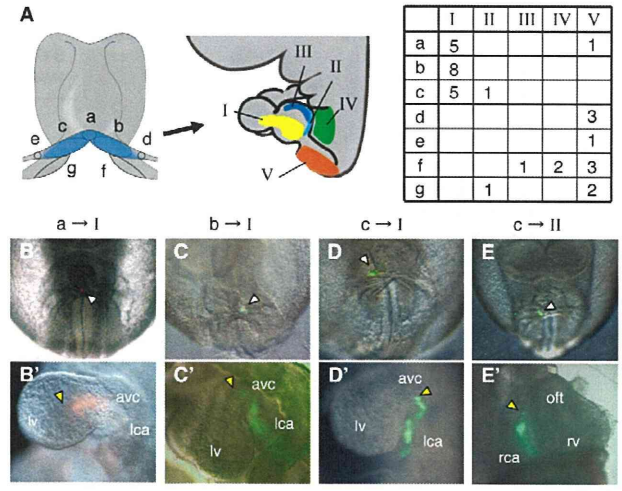

	I	II	III	IV	V
a	5				1
b	8				
c	5	1			
d					3
e					1
f			1	2	3
g		1			2

Fig. 4. PKH fluorescent dye injection into the inflow region. (**A**) Schematics indicating areas of injection (left) and distribution after 30 hours (middle). Table shows the number of embryos observed with dye present in each of the regions I-V following injection at each of the sites a-g. a/b/c, middle/left/right areas within the *Ednra-lacZ/EGFP*-positive region (blue); d/e, areas lateral to b/c; f/g, left/right areas dorsomedial to the *Ednra-lacZ/EGFP*-positive region; I, left lateral wall of the inflow tract; II, right common atrial wall; III, dorsocranial wall of the left common atrium; IV, region around the pharyngeal mesoderm; V, region around the lateral mesoderm. (**B-E′**) Representative results. Dye was injected at the sites indicated (white arrowheads in B-E) and traced after 30 hours (B′-E′). Yellow arrowheads indicate anterior boundaries of dye fluorescence. avc, atrioventricular canal; lca, left common atrium; lv, left ventricle; oft, outflow tract; rca, right common atrium.

detected when *Ednra-EGFP*-positive tails from $Ednra^{EGFP+}$ embryos were transplanted (n=7; Fig. 5C-C″). No fluorescent signals were observed in the left ventricle of wild-type recipients transplanted with a wild-type inflow region (n=7; Fig. 5D-D″). $Ednra^{EGFP+}$ recipients transplanted with the $Ednra^{EGFP+}$ inflow region exhibited strong endogenous EGFP signals in the ventricle, as expected (n=6; Fig. 5E-E″).

To verify further the regional specificity with respect to movement, we transplanted different regions of the E8.25 heart tube, labeled with SYTO16 fluorescent dye, into the inflow region of the heart at the same developmental stage (Fig. 5F). When SYTO16-labeled cells were transplanted into the outflow or ventricular region, no upward movement was detected after 24 hours (n=5 for each; Fig. 5G-G″,H-H″). By contrast, SYTO16-labeled cells were found to distribute along the outer curvature towards the left ventricle after 24 hours in all five embryos transplanted with cells in the inflow region (Fig. 5I-I″). These results strongly support the movement and contribution of *Ednra-lacZ/EGFP*-positive inflow cells to the developing left ventricle.

As indicated by β-galactosidase staining, *Ednra-lacZ/EGFP* was widely expressed in the four chambers after E9.5, raising the possibility that many *Ednra*-negative cells in the early heart tube might become *Ednra*-positive at later stages. To test this idea, we performed explant culture of the ventricular and inflow regions of the E8.25 heart tube separately. At the start of culture, EGFP signals were clearly detectable in the inflow region, but were very low in the ventricle (see Fig. S3 in the supplementary material). After 24 hours, ventricular and inflow regions both demonstrated

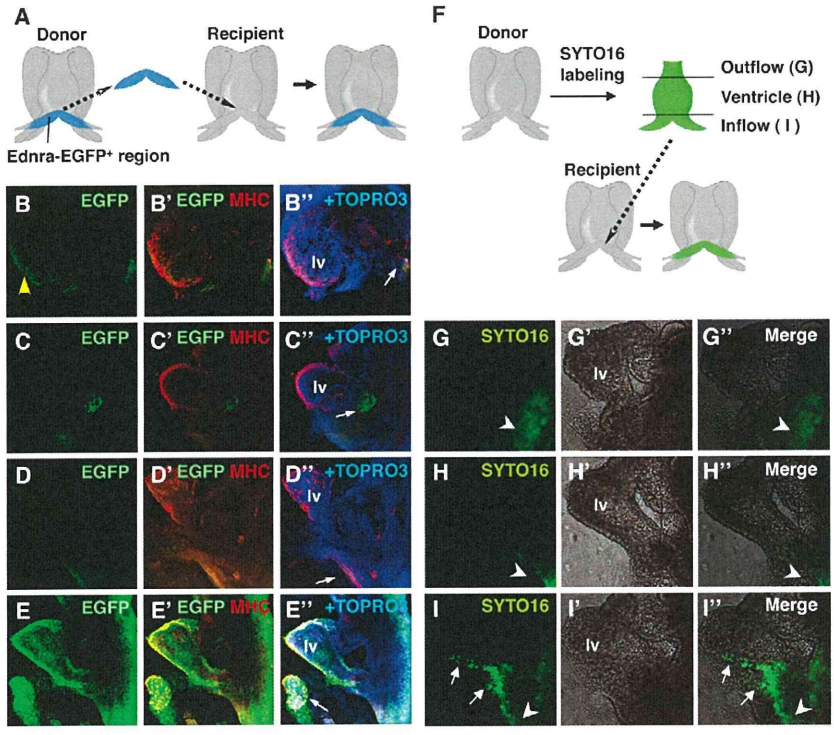

Fig. 5. Transplantation of the ventral inflow region. (**A**) Schematic indicating transplantation of the *Ednra-EGFP*-positive ventral inflow region. (**B-E″**) Representative results 24 hours after transplantation of the inflow region (B-B″,D-E″) or the tail region (C-C″) from $Ednra^{EGFP/+}$ (B-C″,E-E″) or wild-type (D-D″) embryos into the same region of wild-type (B-D″) or $Ednra^{EGFP/+}$ (E-E″) embryos. White arrows, transplants; yellow arrowhead, EGFP signals in the left ventricle (lv). (**F**) Schematic indicating transplantation of SYTO16-labeled heart regions. (**G-I″**) Representative results 24 hours after transplantation of the outflow (G-G″), ventricular (H-H″) and inflow (I-I″) regions. SYTO16 signals (G,H,I) and optical images (G′,H′,I′) are superimposed in G″, H″ and I″. Arrowheads, areas of transplantation; arrows, SYTO16-labeled cells along the outer curvature towards the left ventricle (lv).

intense EGFP signals (see Fig. S3 in the supplementary material). These results suggest that tube-forming cells that are *Ednra* negative at early stages might start to express *Ednra* later.

Defects in ventricular chamber formation in *Ednra*-null mice

In addition to outflow abnormalities as a result of cardiac neural crest defects, some *Edn1*-null embryos from Edn antagonist-treated pregnant mice exhibited ventricular hypoplasia (Kurihara et al., 1995), indicating involvement of Edn signaling in cardiac chamber development. To investigate this further, we revisited the *Ednra*-null phenotype.

At E9.5, when cardiac neural crest cells are not yet seen in the conus arteriosus (Jiang et al., 2000), $Ednra^{lacZ\,EGFP}$ (*Ednra*-null) embryos were obtained at the expected Mendelian ratio (49:102:56 wild-type:heterozygous:null). Of the 43 $Ednra^{lacZ\,EGFP}$ embryos examined, 26 (60%) showed normally developed hearts (Fig. 6A,B). By contrast, 17 $Ednra^{lacZ\,EGFP}$ embryos (40%) showed a gourd-shaped heart with disproportionate chamber sizes (Fig. 6C). These morphological changes indicate that Ednra-mediated signals might be involved in normal growth during chamber formation. To further characterize the *Ednra*-null phenotype, we compared the distribution of β-galactosidase-positive cells in the hearts of $Ednra^{lacZ+}$ and $Ednra^{lacZ\,EGFP}$ embryos at E9.5. β-galactosidase expression in the caudal (posterior) ventricular wall tended to distribute from left to right to a lesser extent in $Ednra^{lacZ\,EGFP}$ embryos than in $Ednra^{lacZ+}$ littermates (see Fig. S4 in the supplementary material). Histological examination revealed that $Ednra^{lacZ\,EGFP}$ embryos often had a poorly developed ventricular wall with a low distribution of β-galactosidase-positive cells (Fig. 6D-G).

Next, we performed BrdU labeling to examine whether the *Ednra*-null phenotype was associated with changes in proliferation. The number of proliferative cells incorporating BrdU was significantly decreased in the compact and trabecular layers of the ventricular wall of *Ednra*-null embryos compared with those of heterozygous $Ednra^{+\,EGFP}$ embryos (Fig. 6H-M). Decreased BrdU uptake in the right ventricle could possibly be explained by low proliferation rates of β-galactosidase-positive cells populated in the caudal (posterior) region (Fig. 2F,G). Indeed, in the right ventricular region, the number of BrdU-labeled cells with a low β-galactosidase-positive population was similar in *Ednra*-null and heterozygous embryos (data not shown). To confirm this, we double stained serial ventricular sections for β-galactosidase activity and phosphohistone H3 (pHH3), a marker of mitosis (Cimini et al., 2003), and counted pHH3-positive cells separately in populations positive and negative for β-galactosidase. The mitotic frequency of β-galactosidase-positive, but not β-galactosidase-negative, cells was decreased in the left and right ventricles of the *Ednra*-null heart (Fig. 6N). Decreased BrdU incorporation in the endocardium of the $Ednra^{lacZ\,EGFP}$ right ventricle is likely to be an indirect effect because the endocardial layer does not express *Ednra-lacZ*. We did not observe differences in the proportion of apoptotic cells between *Ednra*-null and heterozygous or wild-type embryos (data not shown).

Edn1 has been reported to act as a mitogen on cardiomyocytes by stimulating ERK phosphorylation (Sugden, 2003). We therefore examined ERK phosphorylation in E9.5 wild-type, $Ednra^{+\,EGFP}$ and $Ednra^{lacZ\,EGFP}$ hearts. ERK phosphorylation levels were decreased in proportion to the number of *Ednra*-null alleles (Fig. 7A,B). In E9.5 hearts in vitro, stimulation of ERK phosphorylation by Edn1 was abolished by the Ednra antagonist BQ123 (Fig. 7C). Basal ERK phosphorylation was also decreased by BQ123 (Fig. 7D). Taken together, these results suggest that the Ednra signal is involved in myocardial development as a mitogenic factor at early stages. By contrast, no differences in ERK phosphorylation were observed at E10.5 (data not shown), indicating that the negative effect of the *Ednra*-null mutation on myocardial proliferation might be overcome by other factors at later stages.

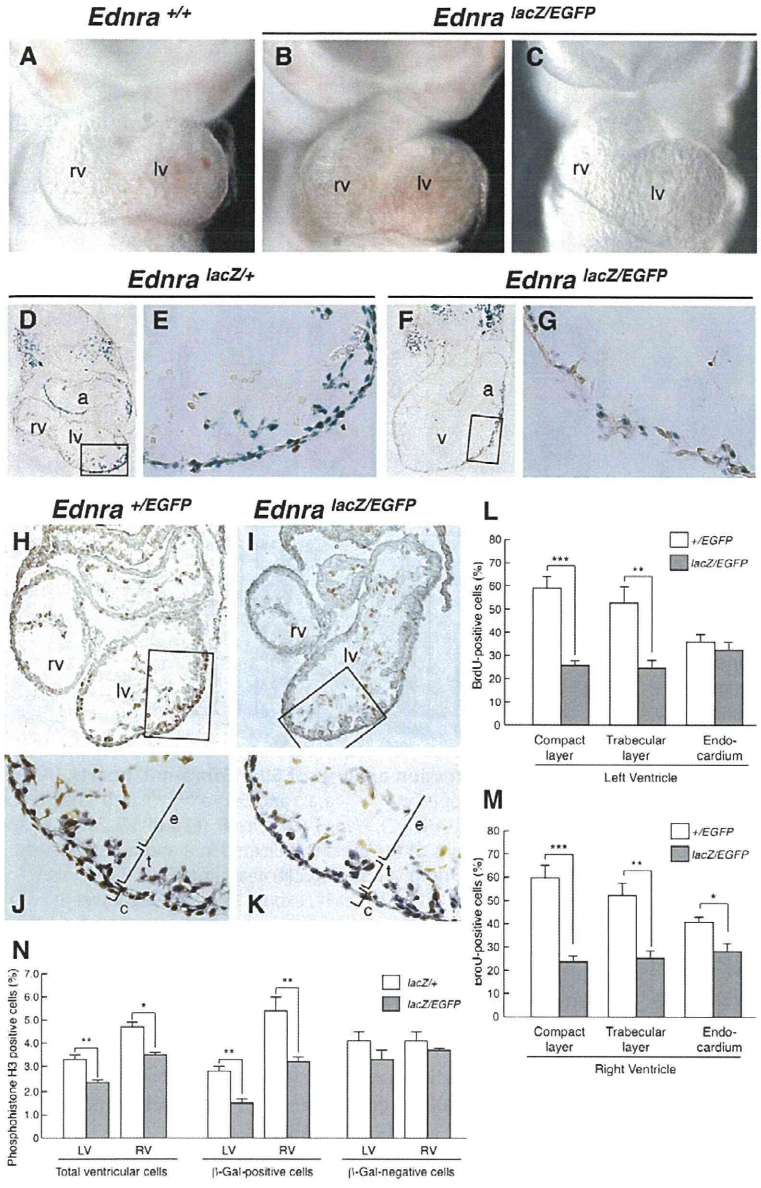

Fig. 6. Morphological, histological and cell proliferation analysis of *Ednra*-null hearts. (**A-C**) Representative wild-type (A) and *Ednra*$^{lacZ/EGFP}$ (*Ednra*-null) (B,C) hearts at E9.5. *Ednra*$^{lacZ/EGFP}$ embryo hearts appear normal (B) or gourd-shaped with disproportionate chamber sizes (C). (**D-G**) Representative transverse sections of E9.25 *Ednra*$^{lacZ/+}$ (D,E) and *Ednra*$^{lacZ/EGFP}$ (F,G) hearts stained for β-galactosidase activity. The boxed areas in D and F are magnified in E and G, respectively. The *Ednra*$^{lacZ/EGFP}$ heart is defective in ventricular wall formation and distribution of β-galactosidase-positive cells. (**H-K**) Representative transverse sections of BrdU-labeled (brown) *Ednra*$^{+/EGFP}$ (H,J) and *Ednra*$^{lacZ/EGFP}$ (I,K) hearts at E9.5. The boxed areas in H and I are magnified in J and K, respectively, after co-staining with Hematoxylin to visualize nuclei (purple). (**L,M**) Quantification of cell proliferation indicated by the ratio of BrdU-positive cells to total cell number in different compartments of the left (L) and right (M) ventricular wall of E9.5 *Ednra*$^{+/EGFP}$ and *Ednra*$^{lacZ/EGFP}$ hearts (n=3 for each). (**N**) Quantification of the percentage of phosphohistone H3-positive cells in the left (LV) and right (RV) ventricles of E9.5 *Ednra*$^{lacZ/+}$ and *Ednra*$^{lacZ/EGFP}$ hearts (n=3 for each) with respect to the numbers of β-galactosidase-positive, β-galactosidase-negative and total cells in three serial sections. Data are presented as mean±s.e.m. *P<0.05, **P<0.01, ***P<0.001. a, atrium; c, compact layer; e, endocardium; lv, left ventricle; rv, right ventricle; t, trabecular layer; v, ventricle.

Changes in T-box transcription factor gene expression in *Ednra*-null hearts

To examine whether the *Ednra*-null mutation affected gene expression in the early developing heart, we performed in situ hybridization for several marker genes on E9.5 *Ednra*$^{+/EGFP}$ and *Ednra*$^{lacZ/EGFP}$ hearts. *Ednra*$^{lacZ/EGFP}$ left ventricles showed decreased expression of *Tbx5* and its downstream gene *Cx40* (Fig. 8A,B), whereas the expression of other chamber myocardium markers such as *ANF*, *Hand1*, *Cited1* and *Mlc2a* was not affected (Fig. 8C-F). Decreased mRNA levels of *Tbx5* and *Cx40*, but not *Hand1*, were also confirmed by quantitative RT-PCR (Fig. 8G). Furthermore, *Tbx5* mRNA levels were increased by Edn1 in excised E9.5 heart explants (Fig. 8H).

The effect of the *Ednra*-null mutation on gene expression patterns was examined further by whole-mount in situ hybridization. In E8.25 *Ednra*$^{+/EGFP}$ and *Ednra*$^{lacZ/EGFP}$ hearts, *Tbx5* expression in the inflow region had a similar pattern to that of *Ednra* (Fig. 9A). At E9.5, *Tbx5* expression was expanded anteriorly towards the left ventricle in *Ednra*$^{+/EGFP}$ embryos (Fig. 9B), as described previously (Bruneau et al., 1999). This anterior expansion of *Tbx5* expression was decreased in *Ednra*$^{lacZ/EGFP}$ hearts, whereas *Tbx5* expression in the posterior (inflow) region was similar to that of *Ednra*$^{+/EGFP}$ embryos (Fig. 9C). By contrast, the *Tbx2*-expressing region, which normally corresponds to the atrioventricular canal (Aanhaanen et al., 2009), was reciprocally expanded in *Ednra*$^{lacZ/EGFP}$ hearts (Fig. 9D,E). *Bmp2* expression in the atrioventricular canal was similar in *Ednra*$^{+/EGFP}$ and *Ednra*$^{lacZ/EGFP}$ hearts (Fig. 9F,G), indicating that the expansion of *Tbx2* expression was independent of Bmp2, an inducer of *Tbx2* in the atrioventricular canal (Kokubo et al., 2007; Yamada et al., 2000). These results indicate that Edn1/Ednra signaling might be involved in the regulation of T-box transcription factor gene expression in early developing hearts.